Title

Tissue driven influences on human NK cell development, function and residence

Journal

The Journal of Immunology, 202(1_Supplement)

ISSN

0022-1767

Authors

Dogra, Pranay
Rancan, Chiara
Ma, Wenji
et al.

Publication Date

2019-05-01

DOI

10.4049/jimmunol.202.supp.129.8

Peer reviewed

Resource

Cell

Tissue Determinants of Human NK Cell Development, Function, and Residence

Graphical Abstract

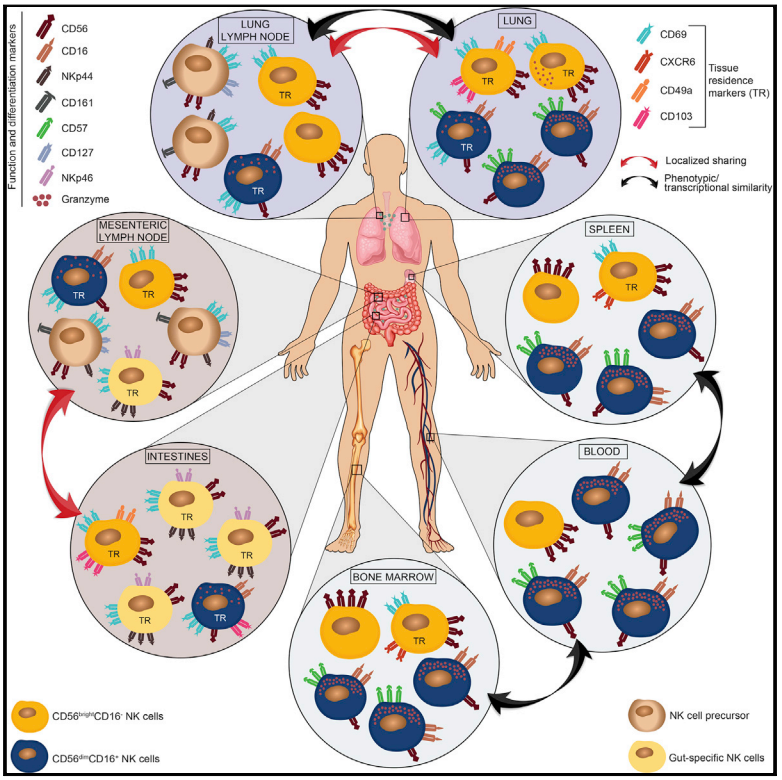

Highlights

- High-resolution map of human NK cells shows tissue-driven distribution across ages
- Differentiated NK cells predominate in blood, bone marrow, spleen, and lungs
- Tissue-resident NK cells exhibit specific adaptations in mucosal and lymphoid sites
- Lymph nodes and intestines are reservoirs for precursor and immature NK cells

Authors

Pranay Dogra, Chiara Rancan, Wenji Ma, ..., Lawrence Fong, Lewis L. Lanier, Donna L. Farber

Correspondence

df2396@cumc.columbia.edu

In Brief

A study of the distribution and function of natural killer cells across various human tissues reveals anatomic control of their development as well as populations that mediate immunosurveillance systemically.

Dogra et al., 2020, Cell *180*, 1–15
February 20, 2020
https://doi.org/10.1016/j.cell.2020.01.022

CellPress

Please cite this article in press as: Dogra et al., Tissue Determinants of Human NK Cell Development, Function, and Residence, Cell (2020), https://doi.org/10.1016/j.cell.2020.01.022

Resource

Cell

Tissue Determinants of Human NK Cell Development, Function, and Residence

Pranay Dogra,[1,2] Chiara Rancan,[3] Wenji Ma,[4] Marta Toth,[5] Takashi Senda,[1,6] Dustin J. Carpenter,[1,6] Masaru Kubota,[1,6] Rei Matsumoto,[1,6] Puspa Thapa,[1,2] Peter A. Szabo,[1,2] Maya Meimei Li Poon,[1] Jacky Li,[3] Janice Arakawa-Hoyt,[7] Yufeng Shen,[4] Lawrence Fong,[3,7] Lewis L. Lanier,[7,8] and Donna L. Farber[1,6,9,10,*]

[1]Columbia Center for Translational Immunology, Columbia University Medical Center, New York, NY 10032, USA
[2]Department of Medicine, Columbia University Medical Center, New York, NY 10032, USA
[3]Division of Hematology/Oncology, Department of Medicine, University of California, San Francisco, San Francisco, CA 94143, USA
[4]Department of Systems Biology, Columbia University, New York, NY 10032, USA
[5]Department of Immunology, Faculty of Medicine, University of Debrecen and Doctoral School of Cell and Immune Biology, University of Debrecen, Debrecen, Hungary
[6]Department of Surgery, Columbia University Medical Center, New York, NY 10032, USA
[7]Parker Institute for Cancer Immunotherapy, University of California, San Francisco, San Francisco, CA 94143, USA
[8]Department of Microbiology and Immunology, University of California, San Francisco, San Francisco, CA 94143, USA
[9]Department of Microbiology and Immunology, Columbia University Medical Center, New York, NY 10032, USA
[10]Lead Contact
*Correspondence: df2396@cumc.columbia.edu
https://doi.org/10.1016/j.cell.2020.01.022

SUMMARY

Immune responses in diverse tissue sites are critical for protective immunity and homeostasis. Here, we investigate how tissue localization regulates the development and function of human natural killer (NK) cells, innate lymphocytes important for anti-viral and tumor immunity. Integrating high-dimensional analysis of NK cells from blood, lymphoid organs, and mucosal tissue sites from 60 individuals, we identify tissue-specific patterns of NK cell subset distribution, maturation, and function maintained across age and between individuals. Mature and terminally differentiated NK cells with enhanced effector function predominate in blood, bone marrow, spleen, and lungs and exhibit shared transcriptional programs across sites. By contrast, precursor and immature NK cells with reduced effector capacity populate lymph nodes and intestines and exhibit tissue-resident signatures and site-specific adaptations. Together, our results reveal anatomic control of NK cell development and maintenance as tissue-resident populations, whereas mature, terminally differentiated subsets mediate immunosurveillance through diverse peripheral sites.

INTRODUCTION

Natural killer (NK) cells are innate lymphocytes that can directly kill target cells without any prior exposure while not damaging healthy "self" cells. Unlike T and B cells that recognize antigen through clonally distributed, somatically rearranged receptors, NK cells recognize their targets through integrating signals from multiple germline-encoded activating and inhibitory receptors that recognize major histocompatibility complex class I (MHC class I) molecules (Colonna et al., 1999; Lanier et al., 1986). In humans, NK cells ($CD3^{-}CD56^{+}$) are relatively abundant, comprising 5%–20% of lymphocytes in blood and other sites (Freud et al., 2017), and play key roles in anti-viral and anti-tumor immunity. NK cells are required for control of acute and persistent viral infections such as Herpesviruses, and in cancer, NK cells promote direct lysis of multiple tumor types, and patrol diverse sites to prevent metastasis (Cerwenka and Lanier, 2001; Imai et al., 2000; Kelly et al., 2002; Morvan and Lanier, 2016; Orange, 2006; Scalzo et al., 2007; Vivier et al., 2012). These multiple aspects of NK cell functionality indicate their dynamic role in immune-mediated protection and homeostasis.

It has become increasingly clear that tissue localization is a critical determinant of the function and *in vivo* role of lymphocytes. Tissue-resident memory T cells (Trm) have been shown in mouse models to populate barrier, mucosal, and peripheral sites following antigen encounter, and are required for optimal protective immunity to pathogens *in situ* (Jiang et al., 2012; Masopust and Soerens, 2019; Muruganandah et al., 2018; Schenkel et al., 2014; Teijaro et al., 2011). In mice and humans, Trm exhibit cell surface phenotypes and transcriptional profiles distinct from circulating memory T cells (Gebhardt et al., 2018; Hombrink et al., 2016; Kumar et al., 2017; Mackay et al., 2016; Szabo et al., 2019), and Trm are the predominant T cell subset in humans (Thome et al., 2014). NK cells also populate multiple tissue sites including liver, lung, skin, kidneys, and bone marrow (BM) and a proportion express Trm markers CD69 and/or CD103 (Freud et al., 2017; Gaynor and Colucci, 2017; Geissmann et al., 2005; Hudspeth et al., 2016; Marquardt et al., 2017; Melsen et al., 2018; Montaldo et al., 2016; Shi et al., 2011; Sojka et al., 2014; Victorino et al., 2015). The role of tissue localization in human NK cell development and function, and how circulating NK cells relate to those in different sites, are not well understood. Human NK cells can be subdivided based on the level of

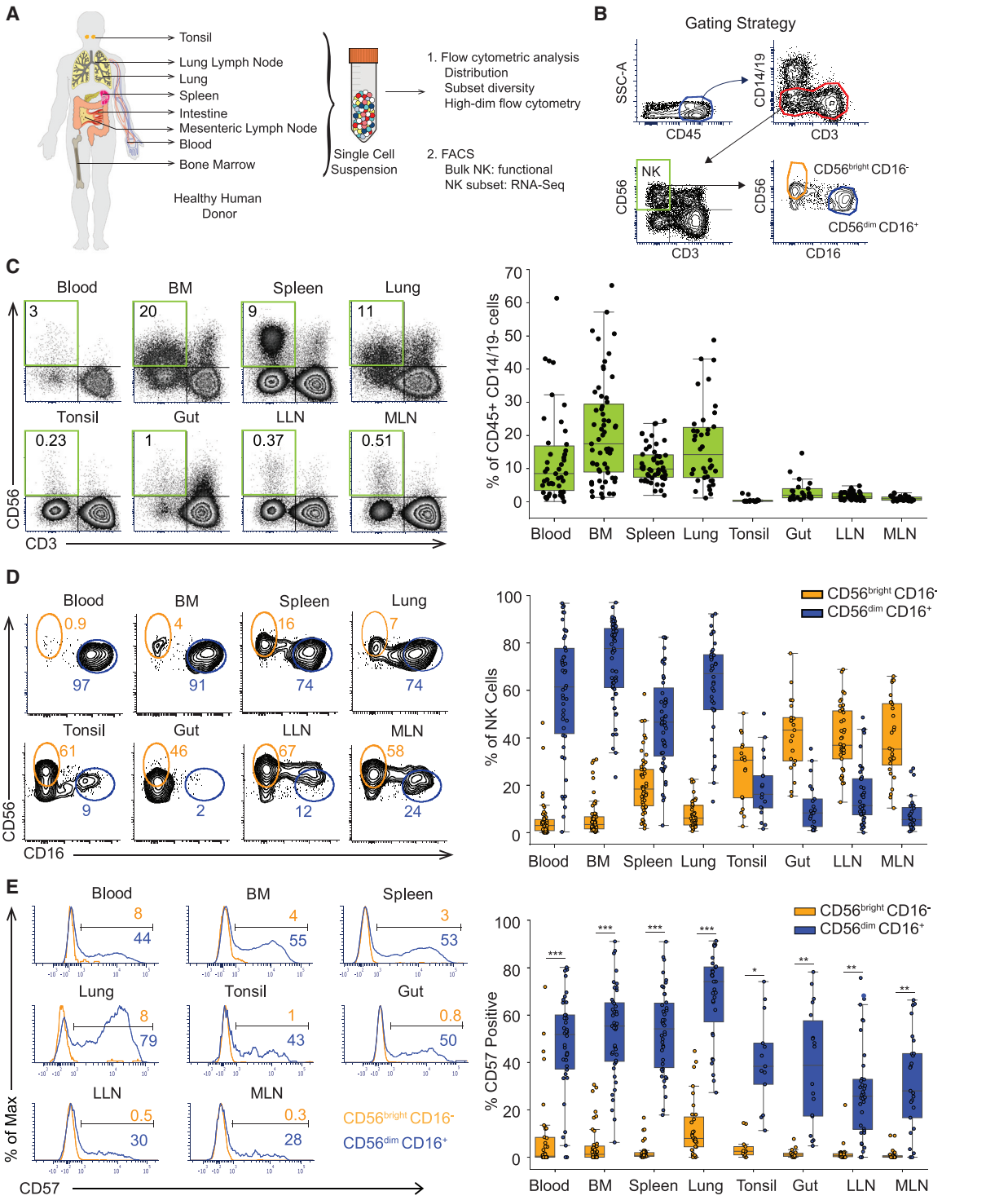

Figure 1. Human NK Cell Subset Distribution Is a Function of Tissue Site

(A) Schematic diagram of the human tissues obtained and experimental workflow presented in this study.

(B) Gating strategy used for identification of NK cells and subsets by flow cytometry for analysis and sorting.

(C) NK cell distribution in different human tissue compartments depicted in representative flow cytometry plots (left, D344) showing NK cell ($CD45^+CD14^-19^-CD3^-CD56^+$) frequency, and boxplots of compiled data from 18–55 donors (right). See also Figure S1A, left panel.

(D) Distribution of $CD56^{bright}CD16^-$ (light orange) and $CD56^{dim}CD16^+$ (blue) NK cell subsets in multiple sites shown in representative flow cytometry plots (left, D337 and D344), and boxplots of compiled data from 18–55 donors for each site (right).

(legend continued on next page)

expression of CD56 and the antibody binding-Fc receptor CD16 into two major subsets with distinct maturation and functional properties (Lanier et al., 1986; Nagler et al., 1989; Yu et al., 2013). $CD56^{dim}CD16^{+}$ NK cells are potent cytolytic effector cells, rapidly secreting pro-inflammatory cytokines (interferon [IFN]-γ, tumor necrosis factor alpha [TNF-α]) and cytotoxic mediators (granzymes and perforin) following receptor-mediated activation. By contrast, $CD56^{bright}CD16^{-}$ NK cells exhibit reduced lytic capacity, although can produce IFN-γ when stimulated with cytokines, interleukin (IL)-12, and IL-18 (Aste-Amezaga et al., 1994; Carson et al., 1994; Cooper et al., 2001; Fehniger et al., 1999). Following stimulation with viruses, cytokines, or haptens, NK cells can also acquire memory-like properties and enhanced functional responses similar to adaptive memory T cells (Cooper et al., 2009; O'Leary et al., 2006; O'Sullivan et al., 2015; Sun et al., 2009, 2010, 2012). Memory-like NK cells responsive to cytomegalovirus (CMV) have been identified in mouse models of MCMV infection and in humans (Arase et al., 2002; Daniels et al., 2001; Dokun et al., 2001; Gumá et al., 2004, 2006; Lopez-Vergès et al., 2011). Understanding the distribution, function, and development of human NK cell subsets across multiple tissue sites, age, and individuals will provide essential insights into their role in immune responses and surveillance.

Here, we investigate how NK cells are distributed across tissues, ages, and individuals and the impact of tissue site on NK development and function, using a human tissue resource we established to obtain blood and multiple tissue sites from individual organ donors spanning nine decades of human life (Carpenter et al., 2018; Gordon et al., 2017; Granot et al., 2017; Kumar et al., 2017). We show that NK cells comprise a sizeable fraction of the lymphocyte compartment in blood, BM, spleen, and lung, where they are predominantly $CD56^{dim}CD16^{+}$; significantly lower frequencies of NK cells populate lymph nodes (LNs), tonsils, and intestines, and are mostly $CD56^{bright}CD16^{-}$. This tissue-intrinsic profile of NK cell frequency, subset distribution, and differentiation states is conserved between diverse individuals over a lifetime. Using high-dimensional transcriptional and phenotypic profiling, we show that precursor and immature NK cells in the lymph nodes and intestines exhibit tissue-resident molecular signatures and site-specific properties, whereas mature and terminally differentiated NK cells have similar effector function and shared gene expression profiles between sites. Our findings reveal tissue-mediated segregation of NK cell development and function and provide a blueprint for how NK cells are seeded, maintained, and surveil tissues across the body.

RESULTS

Tissue-Intrinsic Distribution of Human NK Cell Subsets

To analyze human NK cell distribution, maturation, function, and transcriptional profiles across different anatomic sites and compartments, we obtained blood, BM, secondary lymphoid organs (spleen, lung-draining lymph nodes [LLN], and mesenteric lymph nodes [MLN]), mucosal tissues (lungs, gut [small and large intestine]), and tonsils from human organ donors as described previously (Carpenter et al., 2018; Gordon et al., 2017; Granot et al., 2017; Kumar et al., 2017; Thome et al., 2014; Figure 1A). Tissues were obtained from 60 donors ranging in age from 5–92 years and representing a racially and ethnically diverse population (Table S1). NK cells were distinguished from other lymphocytes and myeloid lineage cells based on gating for $CD45^{+}CD3^{-}CD14^{-}CD19^{-}CD56^{+}$ cells and further delineated into the major NK subsets, $CD56^{bright}CD16^{-}$ and $CD56^{dim}CD16^{+}$ (Figure 1B). The tissue distribution of NK cells among $CD45^{+}CD14^{-}CD19^{-}$ cells was consistent between donors with blood, BM, spleen, and lung having significantly higher frequencies of NK cells (5%–50%) compared to low frequencies (<0.1%–2%) of NK cells in the LNs, tonsil, and gut (Figure 1C and see Figure S1A, left panel for individualized data for each site per donor). BM contained a broader range of NK cell frequencies compared to other sites (Figure 1C), and donors with high NK cell content in BM also showed higher NK frequencies in blood, spleen, and/or lung (Figure S1A, left).

The distribution of $CD56^{bright}CD16^{-}$ and $CD56^{dim}CD16^{+}$ NK cell subsets was also a feature of the tissue site; $CD56^{bright}CD16^{-}$ NK cells predominated in LNs, tonsil, and gut while the majority of NK cells in blood, BM, spleen, and lung were $CD56^{dim}CD16^{+}$ as shown in compiled data (Figure 1D) and for each individual donor (Figure S1A, middle panel). $CD56^{dim}CD16^{+}$ NK cells can be further subdivided into a terminally differentiated subset identified by CD57 expression, resulting from persistent stimulation by antigens or inflammatory signals (Björkström et al., 2010; Lopez-Vergès et al., 2010). The extent of CD57 expression by $CD56^{dim}CD16^{+}$ NK cells varied between sites: substantial frequencies (50%–70%) were $CD57^{+}$ in blood, BM, spleen, and lung, while lower frequencies of CD57-expressing $CD56^{dim}CD16^{+}$ NK cells were present in LNs, tonsils, and gut (Figures 1E and S1A, right). These data further indicate that terminal differentiation of NK cells is more prevalent in sites containing an abundance of $CD56^{dim}CD16^{+}$ NK cells (blood, BM, spleen, and lungs), and excluded from sites such as LN and intestines.

Role of Age, Sex, and CMV Status on NK Cell Subset Distribution

We investigated whether the overall distribution of NK cells or NK cell subsets in tissues varied according to age or CMV serostatus, which are known to affect lymphocyte subset differentiation and immunosenescence (Nikolich-Žugich, 2018; Pawelec and Derhovanessian, 2011). For determining age-associated effects, we performed a correlation analysis of NK cell and subset frequencies as a function of age, revealing consistent, site-specific frequencies of total NK cells and $CD56^{bright}CD16^{-}$:$CD56^{dim}CD16^{+}$ subset ratios from childhood to advanced ages (Figures 2A and 2B). Accordingly, the frequency and tissue distribution of NK cells and $CD56^{dim/bright}$

(E) CD57 expression by $CD56^{bright}$ $CD16^{-}$ (light orange) and $CD56^{dim}CD16^{+}$ (blue) NK cell subsets shown in representative flow cytometry plots (left, D344 and D345) and compiled data from 13–43 donors (right). See also Figure S1A, right panel. Dots on the boxplots show data collected for each individual donor. ***$p \leq 0.001$; **$p \leq 0.01$; *$p \leq 0.05$. Gut refers to both large and small intestines, as we found similar NK cell and subset frequencies for these two sites (Figures S1B and S1C). BM, bone marrow; LLN, lung-draining lymph node; MLN, mesenteric lymph node.

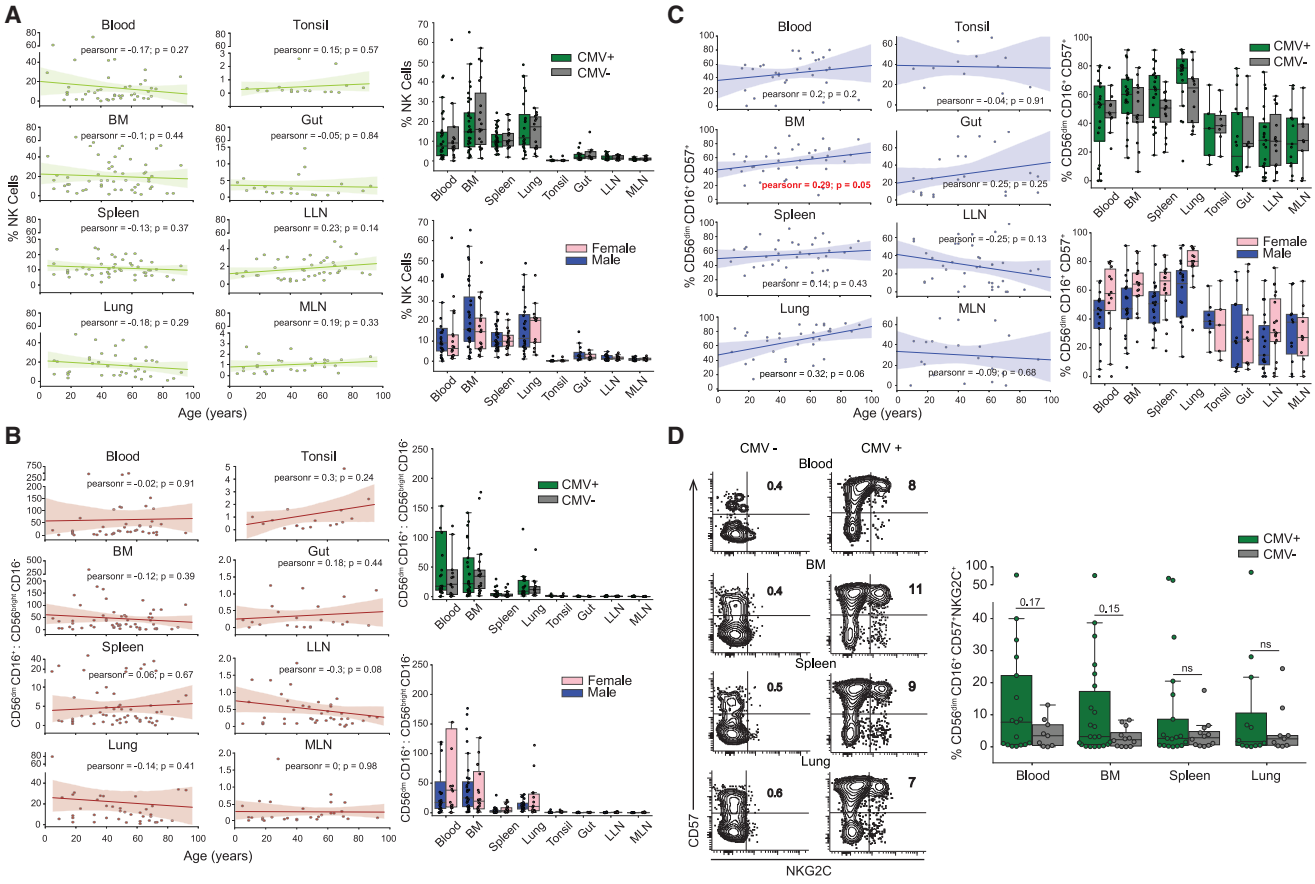

Figure 2. NK Cell Subset Distribution in Tissues Is Independent of Age, Sex, and CMV Serostatus

(A) Scatterplots showing frequency of NK cells in blood and tissue sites as a function of age for each individual donor. The line of best fit was determined by Pearson correlation; the Pearson correlation coefficient for each comparison is designated as "pearsonr" in each plot (left). Right: NK cell frequency in different sites in donors stratified by CMV serostatus (CMV^+, seropositive; CMV^-, seronegative) and sex (male or female).

(B) Scatterplots showing the ratio of $CD56^{dim}CD16^+$:$CD56^{bright}CD16^-$ NK cells in blood and tissue sites as a function of age for each donor, with line of best fit and Pearson coefficient indicated as in (A). See also Figure S1A, middle panel. Right: the ratio of $CD56^{dim}CD16^+$:$CD56^{bright}CD16^-$ NK cells in different sites in donors stratified by CMV serostatus (top) and sex (bottom).

(C) Scatterplots showing the distribution of terminally differentiated NK cells ($CD56^{dim}CD16^+CD57^+$) in blood and tissue sites as a function of age for each donor; the line of best fit and Pearson correlation coefficient indicated in each plot (left). See also Figure S1A, right panel. Right: the distribution of terminally differentiated NK cells in different sites in donors stratified by CMV serostatus (top) and sex (bottom).

(D) Representative flow cytometry plots (left) showing the distribution of CMV-responsive ($CD56^{dim}CD16^+CD57^+NKG2C^+$) memory-like NK cells in a representative CMV-seronegative (CMV^-, D344) and CMV-seropositive donor (CMV^+, D349). Right: boxplots showing compiled distribution of CMV-responsive NK cells from HLA: C1, Bw4/C1, Bw4/C2, and Bw4/C1/C2 CMV^+ (n = 12–17) and CMV^- (n = 9–12) donors, data between the groups was compared using Mann-Whitney U test. See also Figure S2A. Dots on the boxplots show data collected for each individual donor. $^{**}p \leq 0.01$; $^{*}p \leq 0.05$; ns, non-significant. BM, bone marrow; LLN, lung-draining lymph node; MLN, mesenteric lymph node.

subsets did not vary significantly with CMV serostatus or sex of the donor (Figures 2A and 2B), consistent with NK cells being a component of innate immunity. The frequency of terminally differentiated $CD56^{dim}CD16^+CD57^+$ NK cells showed a positive correlation with age in blood, BM, spleen, and lung, which achieved significance in the BM (p = 0.05; lung, p = 0.06), but showed no significant correlation with sex or CMV serostatus (Figure 2C). These results show minimal overt effects of age (over nine decades) and CMV serostatus on the global and site-specific distribution of NK cell subsets, but age-related effects on the accumulation of terminally differentiated NK cells in certain key sites.

To further investigate effects of CMV seropositivity on NK cell subsets across sites, we probed for the presence of memory-like NK cells exhibiting $CD56^{dim}CD16^+CD57^+NKG2C^+$ phenotypes that were previously shown to delineate CMV-responsive NK cells (Hendricks et al., 2014; Lopez-Vergès et al., 2011). CMV-responsive NK cells were detected reliably in blood, BM, spleen, and lung (but not LN, tonsil, or gut) of CMV-seropositive donors but not significantly in CMV-seronegative donors, (Figure 2D). The presence of $CD57^+NKG2C^+$ NK cells was also associated with certain HLA types, with a strong association with HLA-Bw4 and HLA-C1/C2 group antigens (Faridi and Agrawal, 2011; Figure S2A). These data indicate that the

accumulation of CMV-responsive memory-like NK cells occurs in blood and blood-rich sites (BM, spleen, and lung) in a subpopulation of seropositive individuals.

Tissue Site Shapes the Functional Potential of NK Cell Subsets

NK cells acquire granzyme B (GzmB) expression during the maturation process, and GzmB is one of the main cytolytic effector molecules produced by activated NK cells (Fehniger et al., 2007). When stained directly *ex vivo*, there was biased expression of GzmB (40%–80% GzmB$^+$) in CD56^{dim}CD16$^+$ compared to CD56^{bright}CD16$^-$ NK cells across blood and all tissue sites examined (Figure 3A). Between sites, the frequency of GzmB$^+$ in CD56^{dim}CD16$^+$ NK cells is significantly higher in the lung compared to LNs and gut (Figure 3A). GzmB expression by CD56^{dim}CD16$^+$ NK cells is unaffected by age of the donors (Figure S2B). These results suggest conserved functional dichotomies between NK cell subsets across tissues, but tissue-specific variations in cytotoxic potential.

Antibody-mediated crosslinking of CD16 on NK cells elicits antibody-dependent cellular cytotoxicity (ADCC) through association of CD16 with the signaling adaptors FcεRIγ or CD3ζ (Lanier et al., 1989; Wang et al., 2015). The level of FcεRIγ expression is an indicator of ADCC capacity; NK cells that downregulate FcεRIγ and upregulate CD3ζ expression exhibit the most potent ADCC effector function (Lanier et al., 1989; Zhang et al., 2013). In all sites, there was a higher frequency of FcεRIγ$^+$ cells within the CD56^{dim}CD16$^+$ compared to CD56^{bright}CD16$^-$ NK subset (Figure S2C, left panel), consistent with the coordinated expression of FcεRIγ and CD16 in NK cells (Hibbs et al., 1989; Lanier, 2008). However, CMV seropositivity was associated with a slight increase in the frequency of functionally mature (CD56^{dim}CD16$^+$FcεRIγ$^-$) NK cells (Figure S2C, right panel), consistent with the known effects of CMV on NK cells (Lee et al., 2015; Schlums et al., 2015). There were tissue-specific differences in the level of FcεRIγ expression; tonsils, gut, and LN CD56^{dim}CD16$^+$ NK cells express substantially higher levels of FcεRIγ compared to CD56^{dim}CD16$^+$ NK cells in blood, BM, spleen, and lungs (Figure 3B). Site-specific FcεRIγ expression did not vary with age (Figure S2D), suggesting that mature NK cells in blood, BM, spleen, and lung exhibit higher ADCC capacity compared to those in LN and intestines.

NK cells can also elicit effector function in response to cytokine stimulation (Zwirner and Ziblat, 2017). Culturing NK cells from blood, BM, spleen, lung, and LLNs with a cytokine cocktail (IL-12, IL-15, and IL-18) induced IFN-γ production with site-specific differences; BM NK cells had the highest frequency of IFN-γ producers followed by spleen, lung, and blood, with LN having the lowest frequency (Figure 3C). We also tested the functional potential of NK cells activated in the presence of a MHC class I-negative tumor cell line *in vitro* by staining for the expression of lysosomal-associated membrane protein 1 (LAMP-1: CD107a), a marker for degranulation (Alter et al., 2004). NK cells from all the sites showed similar CD107 expression and degranulation potential. Together, these functional analyses indicate site-specific variations in NK cell effector function, particularly in the capacity for cytokine production.

Whole Transcriptome Profiling Uncovers Subset- and Tissue-Specific Features of NK Cells

To identify the molecular basis of differential tissue distribution and functionality between NK cell subsets, we performed whole transcriptome profiling by RNA sequencing (RNA-seq) of CD56^{bright}CD16$^-$ and CD56^{dim}CD16$^+$ NK cells sorted from blood, BM, spleen, lung, and LLN. Analysis of the whole transcriptome identified global signatures of 1,083 genes differentially expressed (DE) between CD56^{bright}CD16$^-$ and CD56^{dim}CD16$^+$ NK cells (702 upregulated and 381 downregulated; Table S2) from these sites. Principal component analysis (PCA) shows subset and tissue-specific distinctions. Along PC2, the transcriptional profile of CD56^{bright}CD16$^-$ NK cells clustered separately from that of CD56^{dim}CD16$^+$ NK cells in all the sites sampled, indicating distinct transcriptional profiles for each subset across sites (Figure 4A; see Figure S3A right for top PC2 loadings). Along PC1 within each subset, blood, BM, and spleen samples clustered together and distinct from lung and LLN samples (Figure 4A). The top genes within the common global signature of DE genes between CD56^{bright}CD16$^-$ and CD56^{dim}CD16$^+$ NK cells from all sites is depicted in the heatmap in Figure 4B and includes genes associated with immune signaling and function as identified by Gene Ontology analysis (Table S3).

The global gene expression differences we identified between CD56^{bright}CD16$^-$ and CD56^{dim}CD16$^+$ NK cells were conserved in all sites, revealing subset-specific profiles consistent with previous studies of NK subsets from single sites (Collins et al., 2019; Koopman et al., 2003; Marquardt et al., 2019; Melsen et al., 2018). Genes upregulated in CD56^{dim}CD16$^+$ NK cells include those associated with effector function (*GZMB*, *GZMH*, *IFNG*), killer cell immunoglobulin-like receptors (*KIR*), and tissue egress and circulation (*S1PR5*, *S1PR1*, *CXCR1*, *CXCR2*, and *CX3CR1*), while CD56^{bright}CD16$^-$ NK cells express elevated levels of genes associated with immune regulation (*CD27*, *TNFSF4*, *TNFSF8*, *TNFSF13*, and *TNFSF13B*) and tissue homing (*CCR7*, *SELL*, *CXCR3*, and *CCR5*) (Figure S3B). CD56^{bright}CD16$^-$ NK cells expressed genes encoding transcription factors involved in cellular stemness and quiescence (Kuo and Leiden, 1999; Zhou et al., 2010) including *LEF1* and *TCF7* (TCF-1), while CD56^{dim}CD16$^+$ NK cells, expressed genes encoding transcription factors associated with terminal differentiation and effector function including *TBX21* (T-bet), *ZEB2*, and *IRF6* (Figure 4C). Differential expression of TCF-1 and T-bet in CD56^{bright}CD16$^-$ compared to CD56^{dim} CD16$^+$ cells in different sites was confirmed by flow cytometry (Figure S3C, top and bottom, respectively). Together, these analyses demonstrate that the core transcriptional identities of CD56^{bright}CD16$^-$ and CD56^{dim}CD16$^+$ NK subsets are maintained in diverse anatomical sites.

NK cell subsets also exhibited site-specific variations in their transcriptional profile. Comparing the transcriptional profiles of tissue CD56^{bright}CD16$^-$ and CD56^{dim}CD16$^+$ NK cells to their counterparts in blood identifies unique DE genes in tissue NK cell subsets (Figure S4A; Tables S4 and S5). Gene set enrichment analysis (GSEA) further reveals subset- and tissue-specific gene expression programs; both NK cell subsets in LLN were enriched for regulatory and tissue retention pathways,

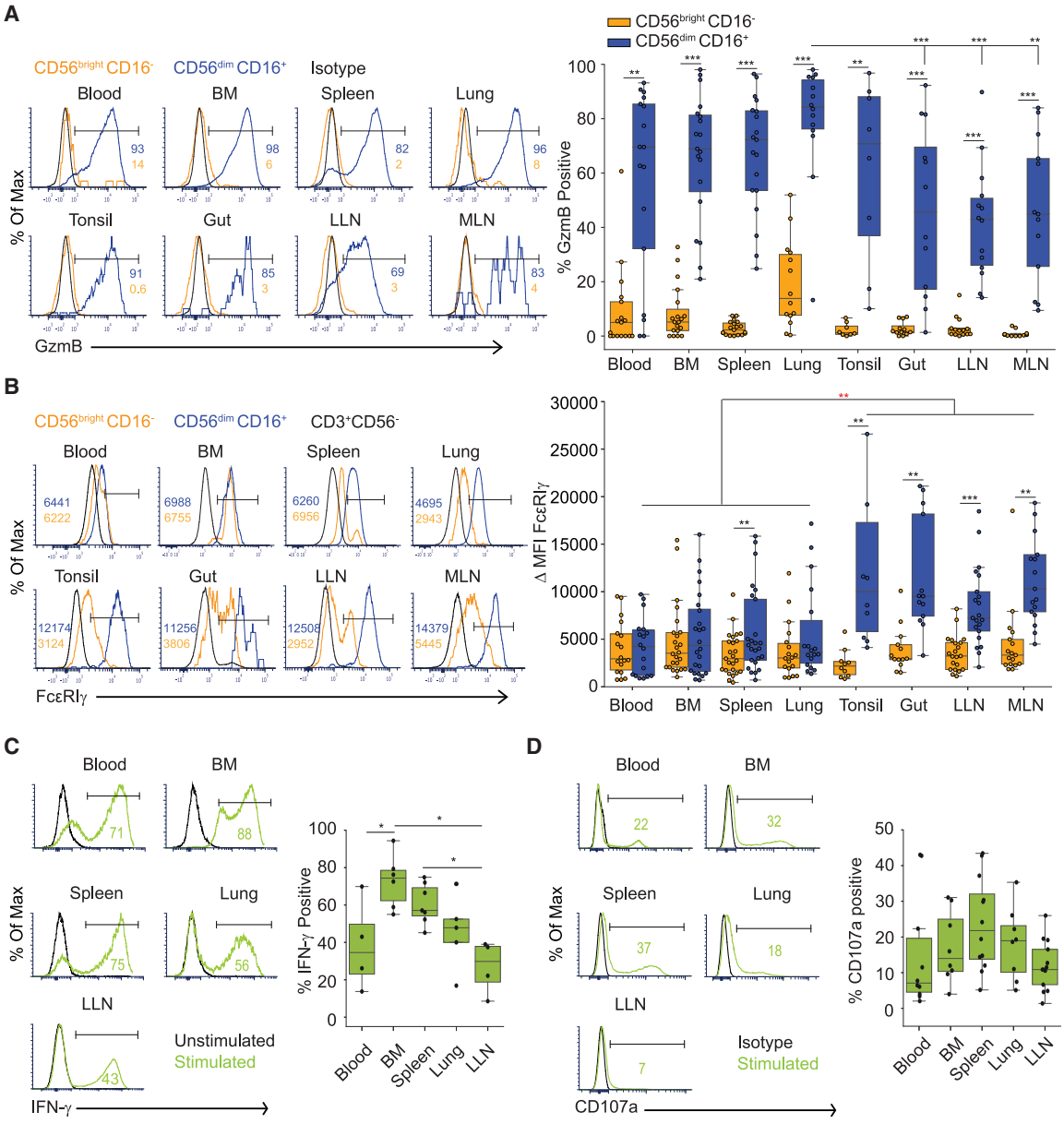

Figure 3. Tissue Localization Shapes the Functionality of NK Cells

(A) Expression of granzyme B (GzmB) by NK cell subsets in different tissue compartments shown in representative histograms (left, D455 and D456) and graphs of compiled frequency of GzmB$^+$ NK cell subsets from 8–19 donors (right). See also Figure S2B.

(B) Expression of the CD16 adaptor molecule FcεRIγ by NK cell subsets in different sites shown in representative histograms (left, D344); numbers in each plot represent median fluorescence intensity (MFI) of FcεRIγ for each subset (light orange, CD56^{bright}CD16$^-$; blue, CD56^{dim}CD16$^+$). Boxplots (right) show ΔMFI FcεRIγ (compiled from 10–25 donors) calculated by subtracting the FcεRIγ MFI of control (CD3$^+$) cells from the FcεRIγ MFI of each NK cell subset. Comparison of ΔMFI from CD56^{dim}CD16$^+$ cells between LN and gut versus blood, BM, spleen, and lung indicated by red asterisk.

(C) IFN-γ secretion following culture of sorted NK cells from indicated sites with cytokines (see STAR Methods) shown as representative histograms (left, D388), and boxplots showing frequency of IFN-γ$^+$ NK cells for each site compiled from 4–7 donors (right).

(D) CD107a expression following activation of NK cells from indicated sites by co-culture with K562 cells for 4 h (see STAR Methods) shown as representative histograms (left, D454), and boxplots showing frequency of CD107a$^+$ NK cells for each site compiled from 8–13 donors (right). Dots on the boxplots show data collected for each individual donor. ***p ≤ 0.001; **p ≤ 0.01; *p ≤ 0.05. BM, bone marrow; LLN, lung-draining lymph node; MLN, mesenteric lymph node.

while in the lung, CD56^{bright}CD16$^-$ NK cells were enriched for cell-adhesion and chemotaxis pathways, and CD56^{dim}CD16$^+$ NK cells were enriched for effector functional programs compared to other sites (Figures S4B and S4C). Moreover, PCA analysis for the individual subsets revealed more site-specific differences among CD56^{bright}CD16$^-$ NK cells compared to CD56^{dim}CD16$^+$ NK cells. In particular, the transcriptional profile of CD56^{bright}CD16$^-$ NK cells from blood, BM, and spleen

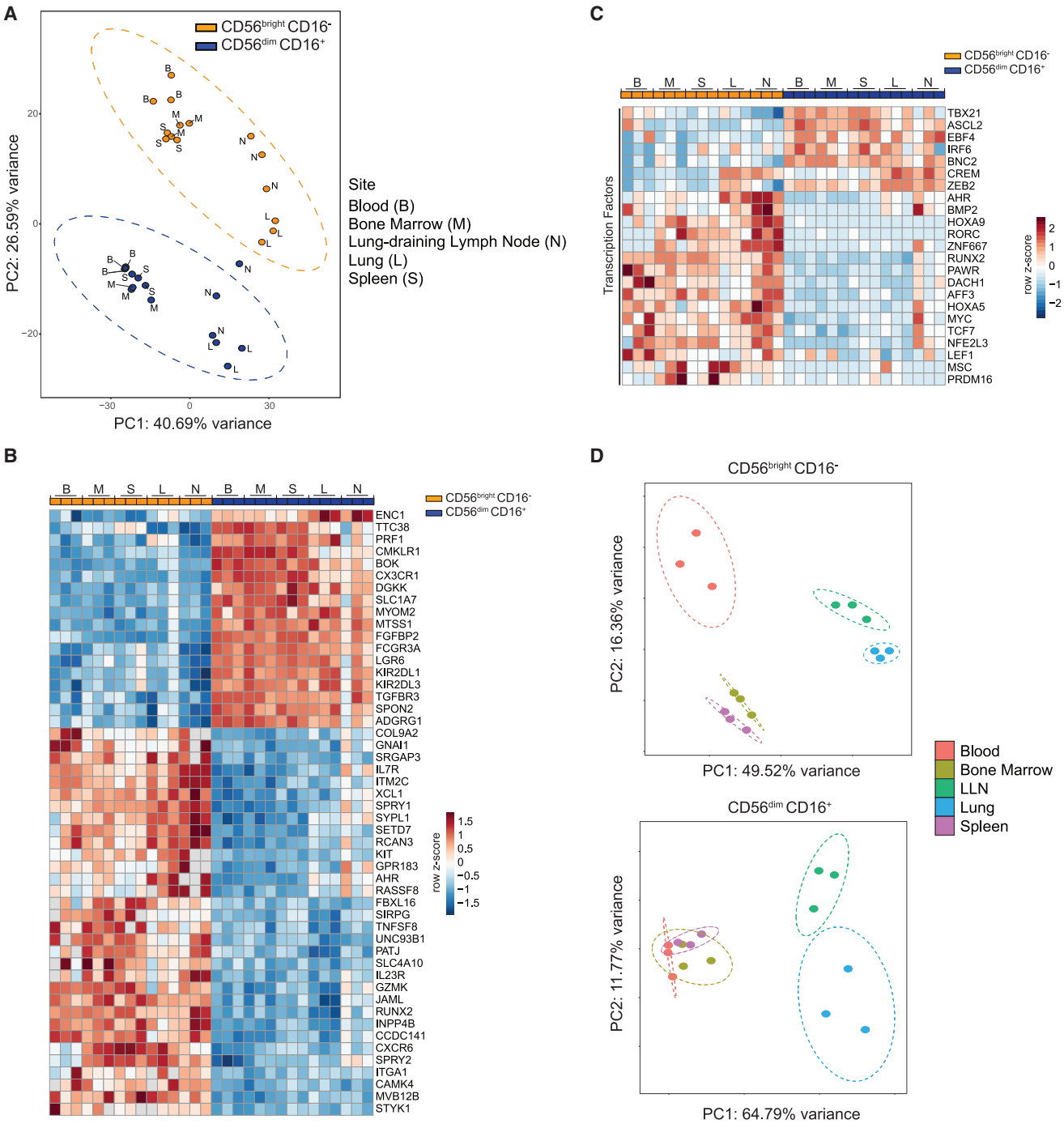

Figure 4. Transcriptional Analysis of CD56^{bright}CD16^{-} and CD56^{dim}CD16^{+} NK Cells across Sites

(A) PCA plot generated from top 500 differentially expressed (DE) genes between CD56^{bright}CD16^{-} and CD56^{dim}CD16^{+} NK cell subsets isolated from 5 sites (blood, BM, spleen, lung, and lung-draining LN). See Table S2 for complete gene list.

(B) Heatmap of top 50 globally DE genes between CD56^{bright}CD16^{-} and CD56^{dim}CD16^{+} NK cell subsets from all sites.

(C) Heatmap showing the top DE transcription factors between CD56^{bright}CD16^{-} and CD56^{dim}CD16^{+} NK cells from all sites.

(D) PCA plot for CD56^{bright}CD16^{-} (top) and CD56^{dim}CD16^{+} (bottom) NK cells isolated from five sites. Each dot in the PCA plots is a separate donor sample, and ellipses around samples indicate 95% confidence ellipses (see STAR Methods). B, blood; M, bone marrow; S, spleen; L, lung; N/LLN, lung-draining lymph node. See also Figures S3 and S4.

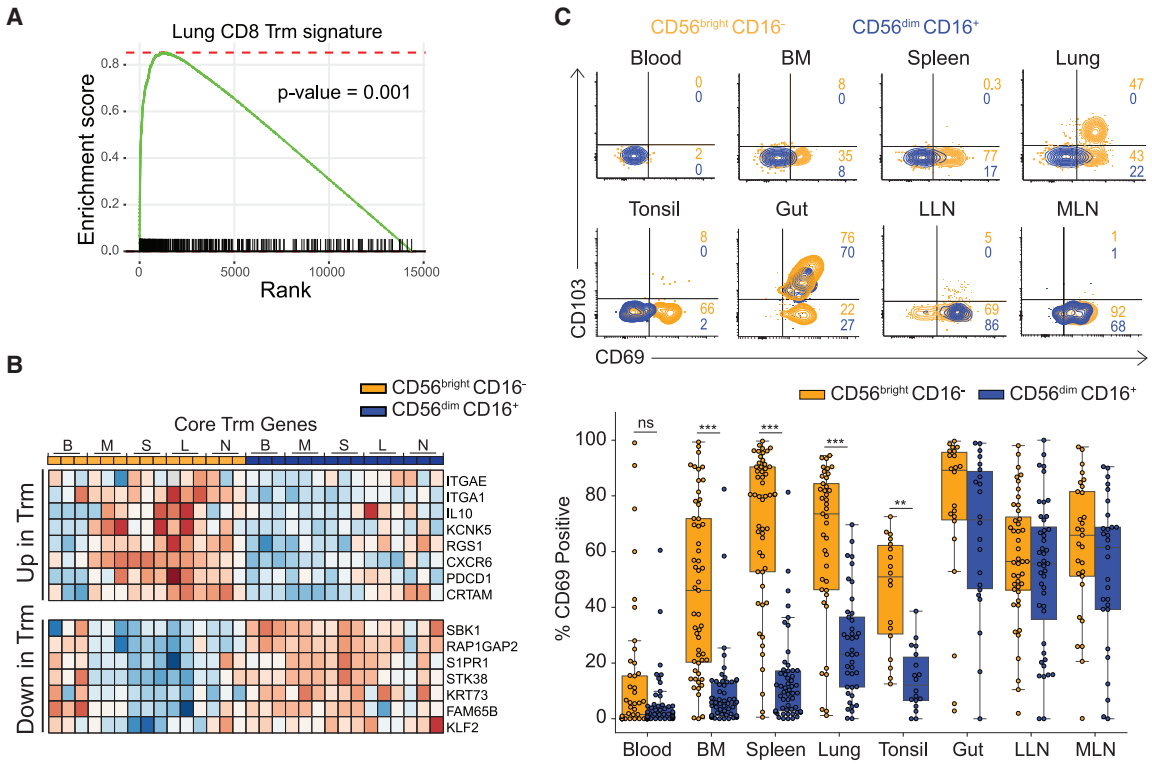

Figure 5. Tissue Residence Profile of CD56^{bright}CD16^{-} NK Cells

(A) GSEA plot showing the enrichment of core tissue resident-memory T (Trm) cell genes within CD56^{bright}CD16^{-} NK cells from all tissue sites. See also Figure S5A.

(B) Heatmap showing the expression of select core Trm signature genes differentially expressed in tissue CD56^{bright}CD16^{-} NK cells and not expressed in blood CD56^{bright}CD16^{-} or CD56^{dim}CD16^{+} NK cells in all sites.

(C) Cell surface expression of canonical tissue residence markers CD69 and CD103 on CD56^{bright}CD16^{-} (light orange) and CD56^{dim}CD16^{+} (blue) NK cell subsets in different tissue compartments shown in representative flow cytometry plots (top, D337 and D351) and boxplots showing percent CD69^{+}NK cells within each subset in different tissue compartments compiled from 18–40 donors. Dots on the boxplots show data collected for each individual donor. See also Figure S5B. ***p ≤ 0.001; **p ≤ 0.01. B, blood; M/BM, bone marrow; S, spleen; L, lung; N/LLN, lung-draining lymph node; MLN, mesenteric lymph node.

clustered separately on the PCA plot, whereas CD56^{dim}CD16^{+} NK cells from these sites clustered together (Figure 4D). In contrast, the transcriptional profile of both CD56^{bright}CD16^{-} and CD56^{dim}CD16^{+} NK cell subsets in the lung and LLN were distinct from the corresponding subsets in blood and other tissue sites (Figure 4D) and showed increased sharing of transcriptional programs compared to these sites (Figures S4D and S4E). These results suggest a common origin for NK cells that populate the lung and the LLN. Taken together, our findings reveal that although NK cell subset transcriptional identity is preserved across sites, tissue localization drives further subset-specific transcriptional programs in NK cells.

CD56^{bright}CD16^{-} NK Cells in Tissues Exhibit a Tissue-Resident Gene Expression Signature

We hypothesized that the tissue-adapted gene expression programs of CD56^{bright}CD16^{-} NK cells derives from their residence in tissues. GSEA comparing the transcriptome of CD56^{bright}CD16^{-} NK cells to the Trm gene signatures we previously identified in human tissue sites (Kumar et al., 2017) revealed significant enrichment of core signature genes of human lung and spleen CD8^{+}Trm within CD56^{bright}CD16^{-} NK cells in tissues (Figure 5A). Core Trm gene expression signatures including upregulation of the integrin *ITGAE* (CD103), *ITGA1*, and the chemokine receptor *CXCR6* and downregulation of tissue egress molecules *S1PR1* and *KLF2* (Kumar et al., 2017), distinguished tissue CD56^{bright}CD16^{-} NK cells from CD56^{bright}CD16^{-} NK cells in blood and CD56^{dim}CD16^{+} NK cells in all sites (Figure 5B). There were also site-specific variations in the extent of expression of certain core genes incusing *CXCR6*, *ITGA1*, and *ITGAE* (Figure S5A), suggesting tissue-specific effects on the establishment of residency programs.

The expression of canonical TRM surface markers CD69 and CD103 by tissue NK cells showed subset- and site-specific variations. In BM, spleen, lungs, and tonsils, CD69 was expressed by significantly higher frequencies (35%–90%) of CD56^{bright}CD16^{-} compared to CD56^{dim}CD16^{+} NK cells; however, in gut and LN, CD56^{bright}CD16^{-} and CD56^{dim}CD16^{+} NK cell subsets exhibited comparable CD69 expression (Figure 5C). In mucosal sites (lungs, intestines) substantial frequencies of CD69^{+} NK cells co-expressed CD103 (Figure 5C). The frequency and distribution of CD69 expression by CD56^{bright}CD16^{-} NK cells

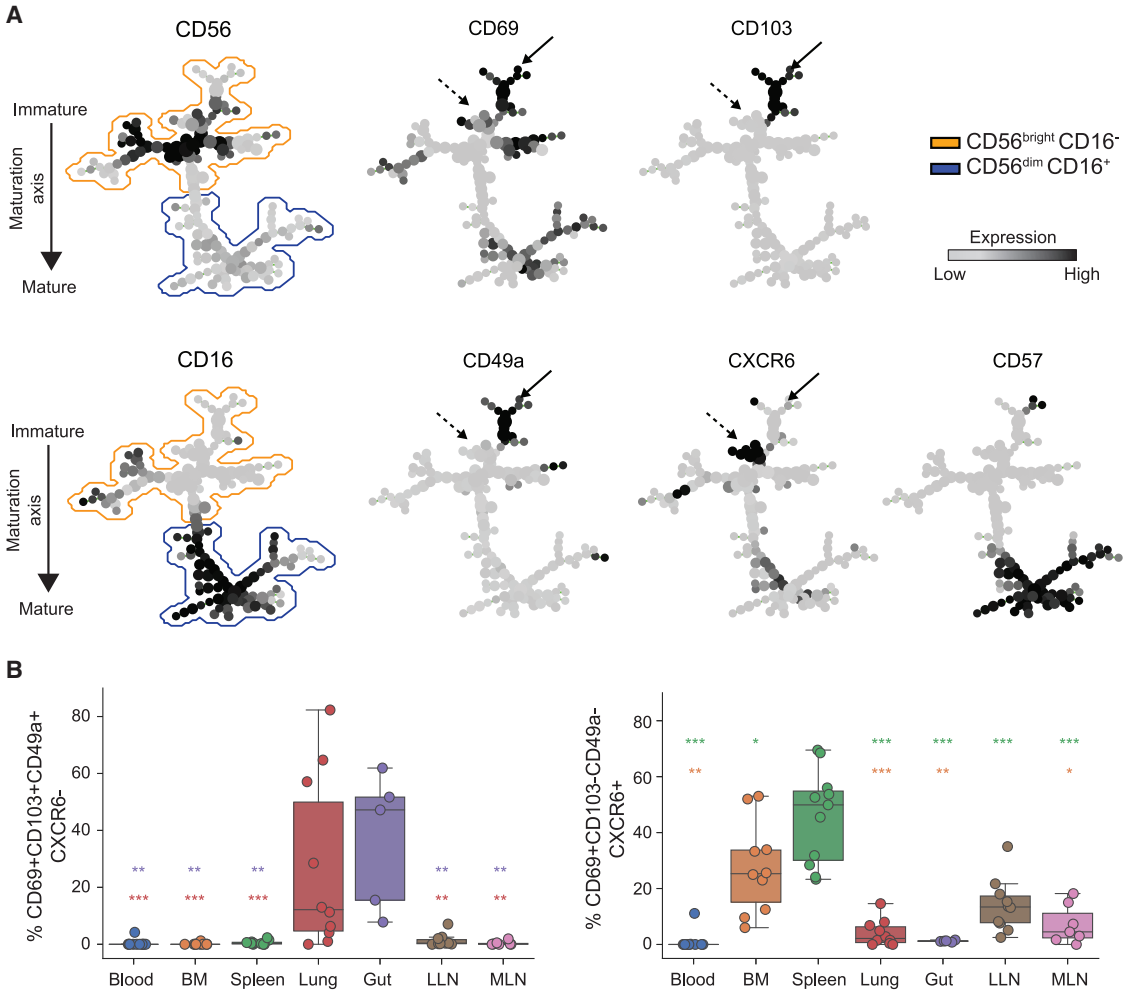

Figure 6. Heterogeneity of Tissue Resident NK Subsets across Sites

(A) Representative SPADE plots of NK cells from blood, BM, spleen, lung, gut, LLN, and MLN stained with tissue-residence markers. The two plots on the left show the distribution NK cells along the maturation axis. The plots on the right show the expression and distribution of select residence markers and marker for terminal differentiation on NK cells along the maturation axis. Solid black arrow identifies CD103- and CD49a-expressing NK cell cluster and dashed black arrow identifies the CXCR6-expressing NK cell cluster. See also Figure S5C.

(B) Boxplots showing the distribution of $CD69^{+}CD103^{+}CD49^{+}CXCR6^{-}$ (left) and $CD69^{+}CD103^{-}CD49a^{-}CXCR6^{+}$ (right) $CD56^{bright}CD16^{-}$, NK cells in indicated tissue sites compiled from 5–10 donors. Dots on the boxplots show data collected for each individual donor. Red asterisk, comparison between lung and tissue site; purple asterisk, comparison between gut and tissue site; orange asterisk, comparison between BM and tissue site; green asterisk, comparison between spleen and tissue site. ***$p \leq 0.001$; **$p \leq 0.01$; *$p \leq 0.05$. BM, bone marrow; LLN, lung-draining lymph node; MLN, mesenteric lymph node.

in tissues was not altered with age (Figure S5B), suggesting that tissue residence is an intrinsic property. These findings show that $CD56^{bright}CD16^{-}$ NK cells exhibit features of tissue residency in multiple sites, whereas $CD56^{dim}CD16^{+}$ NK cells bear signatures of circulating cells in blood, BM, and spleen, but can adopt resident phenotypes in LN and mucosal sites.

Tissue-Specific Properties and Heterogeneity of Tissue-Resident Cells

We assessed coordinate expression of key tissue residency markers CD69, CD103, CD49a, and CXCR6 (Kumar et al., 2017; Peng and Tian, 2017) to further investigate site-specific differences as suggested by the transcriptional data (Figure S5A) and define potential heterogeneity of putative tissue-resident NK (trNK) cells in different anatomical sites. Spanning-tree progression analysis of density-normalized events (SPADE) (Qiu et al., 2011) projection of NK cells from blood, BM, spleen, lung, gut, LLN, and MLN identified distinct branches of $CD56^{bright}CD16^{-}$ NK cells that exhibit site-specific variations in expression of tissue-resident markers, consistent between five individual donors (Figures 6A and S5C). CD69 expression was detected in the majority of $CD56^{+}$ NK cells, except for a specific branch of cells expressing the highest levels of CD56 that lack CD69 (Figures 6A and S5C), and may represent a circulating subset of immature NK cells. Other tissue-resident markers were differentially expressed; CXCR6 expression was exclusive

of CD103 and CD49a expression and was mostly confined to BM, spleen, and LNs, while CD49a and CD103 were expressed together on subsets of CXCR6^{-}CD69^{+}NK cells in the lung and gut (Figures 6A, 6B, and S5C). These site-specific variations in CXCR6, CD49a, and CD103 expression in trNK subsets are consistent with variations in expression of the corresponding genes between sites (Figures 5B and S5A) and reveal tissue-specific segregation of trNK subtypes.

Maturation and Developmental States of NK Cells across Tissues

NK cells undergo progressive development from CD56^{bright} into CD56^{dim} NK cells, involving expression of specific receptors associated with distinct maturation states (Abel et al., 2018; Scoville et al., 2017). For example, CD161 is one of the earliest markers expressed on NK cells during maturation from CD34^{+} hematopoietic stem cell precursors; inhibitory and activating receptors CD94/NKG2A, NKp46, NKp44, CD160, and NKG2D can be variably expressed in different maturation states, while expression of CD16 and multiple KIRs mark mature NK subsets, and CD57 indicates terminal differentiation. In order to trace the developmental origin of NK cell subsets in tissues, we implemented a high-dimensional flow cytometry panel incorporating multiple NK functional and developmental markers (Figure S6; Key Resources Table).

Force-directed clustering analysis of NK marker expression data from seven sites (blood, BM, spleen, lung, gut, LLN, and MLN) of five individuals generated 15 distinct NK cell clusters that were consistent between donors (Figures 7A and 7B; Table S6). There were 7 clusters within the CD56^{bright} population: cells in clusters 1 and 2 express CD56, CD127, and CD161. Cluster 1 cells also express very low levels of activating receptor NKp44 and resemble NK-precursor-like cells described previously (Di Santo and Vosshenrich, 2006; Freud et al., 2005; Scoville et al., 2017), while cluster 2 cells exhibit increased expression of CD56 and NKG2A (Figures 7A and 7C). The remaining CD56^{bright} cells in clusters 3–7 lack CD127 expression and show reduced NKp44 expression (except in cluster 3) but express the activating receptor NKG2D, the inhibitory receptor NKG2A, and variable levels of NKp46, CD160, and CD161 (Figures 7A, 7C, and S6). CD56^{dim}CD16^{+} (mature) NK cells partition into 8 clusters (clusters 8–15) showing a progressive loss of CD160, CD161, NKp46, NKG2D, and NKG2A expression, and concomitant upregulation of CD57 and KIRs along the maturation axis (Figure 7A). The more mature CD56^{dim} NK cells (clusters 13,14,15) resemble terminally differentiated NK cells exhibiting upregulated expression of CD57, KIRs, and downregulation of CD27 (Figures 7A and 7C). Therefore, multiple states of NK development and differentiation can be detected across blood and tissues.

The distribution of NK cell maturation states was site-specific. BM and spleen contained the most heterogeneous composition of NK cells, comprising multiple maturation states, including precursor NK cells (clusters 1 and 2), three immature subsets (clusters 5–7), and all eight clusters that defined the mature CD16^{+} population (Figure 7D). Conversely, NK subsets in blood and lung consisted largely of mature and terminally differentiated states, particularly in the lung where clusters 13–15 predominated. By contrast, immature subsets populating LLN and MLN contained the two precursor subsets (CD56^{bright}CD127^{+}CD161^{+}) along with lower frequencies of five immature NK cell states (clusters 3–7) (Figure 7D; Table S6). Although CD127 is also a marker for innate lymphoid cells (ILC) (Vivier et al., 2018), we did not detect substantial frequencies of CD127^{+} RORγt^{+} ILC3s (Li et al., 2018; Yudanin et al., 2019) among CD56^{+} cells from LLN, gut, and spleen or the other sites examined (Figure S7A). Moreover, the transcriptional profile of spleen and LLN NK cell subsets (Figure 4) was distinct from that of human ILC subsets in different sites recently reported (Yudanin et al., 2019; Figure S7B). Together, these data provide further evidence that the prevalent NK populations in LN likely represent precursor NK cells and NK subsets maintained in less differentiated states compared to other peripheral sites.

Last, we identified only two NK cell states in the gut (clusters 3 and 4) that were not found in the other sites except for low frequencies, specifically in the gut-draining MLN, and not in LLN. Cluster 3 cells exhibited a distinct NKp44^{+}NKp46^{+}CD160^{+}CD294^{lo}NKG2A^{-} phenotype, whereas cluster 4 cells lacked expression of NKp44, NKp46, and CD160, but exhibited upregulated expression of CD85j, an MHC class I-binding immunoglobulin-like molecule with inhibitory activity (Colonna et al., 1997). These distinct NK cell subsets appear to be specific or enriched within intestinal sites (and intestinal LN) because in the donors from whom we did not obtain intestinal tissues (donors 1–3; Figure 7B), these clusters were not observed. This high-dimensional analysis of NK cells across multiple tissues within individual donors demonstrate tissue-specific distribution of developmental and functional states of NK cells and identifies the LN and intestines as reservoirs for specific populations of precursor and immature NK cells, respectively.

DISCUSSION

We reveal here the role of tissue localization in the development, function, and transcriptional program of NK cells, critical innate lymphocytes that mediate control of viral infections and tumors. Analysis of primary and secondary lymphoid organs as well as mucosal sites obtained from 60 organ donors shows that the tissue distribution of human NK cells and major NK cell subsets is a function of the tissue site and is unaffected by age, sex, and CMV serostatus. NK cells are most abundant in blood, BM, spleen, and lung, which are dominated by mature (CD56^{dim}CD16^{+}), terminally differentiated (CD56^{dim}CD16^{+}CD57^{+}), and CMV-responsive (CD56^{dim}CD16^{+}CD57^{+}NKG2C^{+}) NK cell subsets with high effector function. Significantly lower frequencies of NK cells are found in LN, tonsils, and intestines comprising mostly immature (CD56^{bright}CD16^{-}) subsets with reduced effector capacity, which exhibit features of tissue-resident lymphocytes and tissue-specific adaptations. Moreover, developmental lineages of NK cells exhibit site-specific distribution and phenotypes; NK cell precursors and immature tissue-adapted subsets localize in LN and intestines; spleen and BM contain all developmental stages, whereas lung has prevalent mature and terminally differentiated NK cells. Together, our results

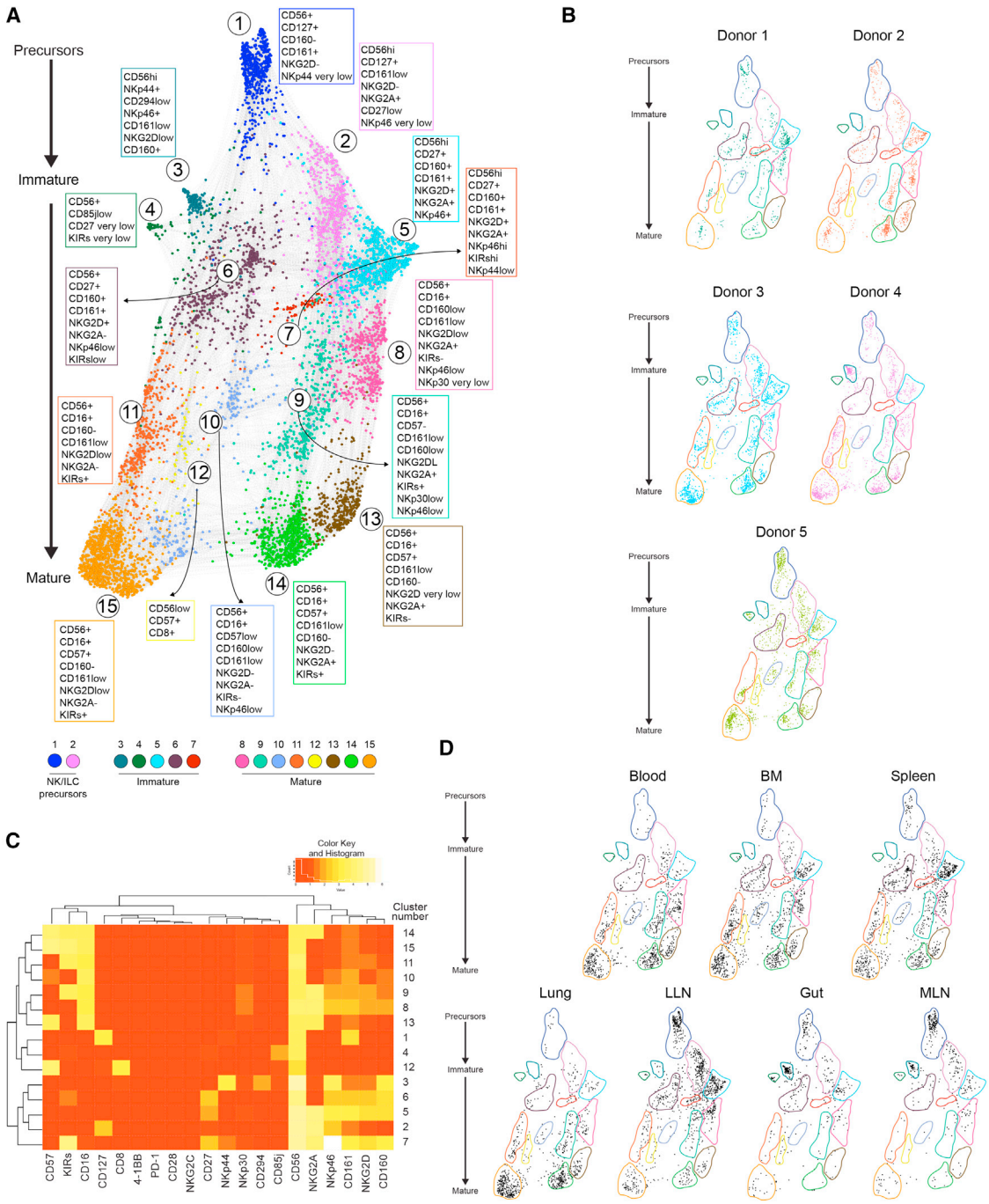

Figure 7. High-Dimensional Flow Cytometry Profiling Identifies Tissue-Specific Patterns of NK Development and Maturation

NK cells from blood, bone marrow (BM), spleen, lung, gut, lung-draining LN (LLN), and mesenteric LN (MLN) were stained with the high-dimensional antibody panel specific for multiple NK cell maturation and function markers (see STAR Methods). See also Figure S6.

(A) Force-directed plot showing the relationship between different NK cell communities identified by multi-dimensional analysis (data compiled from 5 donors). Each node is an aggregation of similar cells resulting from downsampling of data, and collection of similar colored nodes forms 15 distinct NK cell clusters. Colored text boxes show markers used to differentiate each cluster (1–15).

(B) Plots showing the distribution of NK cell communities across the five donors.

(C) Heatmap showing the differential expression of cell surface markers used for clustering and community identification in the multi-dimensional analysis in (A).

(D) Scatterplots showing distribution of NK cell states in each tissue among the clusters identified by multi-dimensional analysis. For (B) and (D), colored shapes delineate boundaries corresponding to each cluster identified in (A).

provide evidence for tissue-driven segregation of NK cell development, function, and immunosurveillance.

Our tissue resource enables assessment of immune cells across sites within and between individuals, for unambiguous determination of attributes that are tissue-intrinsic versus those that vary due to age, sex, or between individuals. As shown here, the distribution of NK cells and subsets and their intrinsic function are features of the tissue site and are remarkably consistent between donors independent of age or sex, consistent with their role as an innate immune cell. Notably, the majority of NK cells localize in the blood, and blood-rich sites such as BM, spleen, and lungs where they are largely $CD56^{dim}CD16^{+}$ cells with high effector capacity—a subset predominance consistent with previous studies of human NK cells (Castriconi et al., 2018; Freud et al., 2017; Robertson and Ritz, 1990). Terminally differentiated and memory-like NK cells, including CMV-responsive NK cells, also predominate in these blood-rich sites. By contrast, NK cells are present only at low frequencies in LNs, tonsils, and throughout the GI tract where they are predominantly $CD56^{bright}CD16^{-}$ cells, while mature and terminally differentiated NK cells are largely excluded from these sites. This compartmentalization of NK cell subsets may occur due to seeding of distinct subsets directly from the BM or differential migration of NK populations during maintenance.

We show here that $CD56^{bright}CD16^{-}$ NK cells in lymphoid and mucosal tissues exhibit key transcriptional and functional features of Trm cells (Kumar et al., 2017; Mackay et al., 2016; Masopust and Soerens, 2019). In contrast to T cells where tissue residency is acquired during differentiation to memory T cells, tissue residency in NK cells is a feature of the less differentiated subset, consistent with recent results in human BM and lung (Marquardt et al., 2019; Melsen et al., 2018). By contrast, $CD56^{dim}CD16^{+}$ and memory-like NK cells exhibit features of circulating cells and are prevalent in blood-rich sites. We also show that trNK cells exhibit site-specific transcriptional and phenotypic adaptations. In particular, $CD56^{bright}CD16^{-}$ cells from LN and lung were transcriptionally distinct compared to BM and other sites, due in part to differential expression of residency markers CD49a, CD103, and CXCR6 and multiple chemokine and homing receptors. Together, these data provide strong evidence for differential requirements for NK cell homing and/or retention in distinct tissue sites.

The diversity in NK cell phenotypes is driven by the differential expression of developmentally regulated receptors, which also govern the functional responsiveness of NK cells (Colonna et al., 1999; Lanier et al., 1986; Pegram et al., 2011). Our high-dimensional analysis of multiple NK cell lineage markers revealed tissue-specific patterns of NK development and function. At the earliest differentiation states, $CD127^{+}NKp44^{low}$ NK precursor-like cells were predominant in LNs and were similar to those identified as stem cell-derived and thymus-derived NK cells (Freud et al., 2005; Luther et al., 2011; Vosshenrich et al., 2006). LN also contain additional immature subsets ($CD16^{-}CD160^{low}KIR^{low}$), which express transcripts encoding chemokines (e.g., *XCL1*, *XCL2*, and *CCL5*) for recruitment of lymphocytes and myeloid cells (Bottcher et al., 2018), and resemble the NK2 subset recently described (Crinier et al., 2018). Intestines also harbor immature subsets, but maintain predominantly two specific types not found in blood or other tissues that are also found in gut-associated LN. One of the intestine-specific subsets exhibits co-expression of NKp44 and NKp46 and may resemble NK cell phenotypes associated with inflammatory bowel disease (Poggi et al., 2019). Interestingly, the blood, BM, and spleen contain a range of NK cell subsets and differentiation states expressing a range of KIRs, NCRs, and activating receptors, consistent with previously defined heterogeneity among blood NK cells (Bengsch et al., 2018; Horowitz et al., 2013), while lung is enriched in highly differentiated NK cells.

Together, our results suggest a model for anatomic control of NK cell development and function. Specifically, precursor and immature NK cells are seeded into LNs and intestines where they take up residence, and these sites may therefore serve as reservoirs for NK cell maintenance. Activation and differentiation of NK cells triggers dispersal into other sites including spleen, blood, and lung, where they conduct immunosurveillance and mediate effector function. In this way, NK cells control virus infections and tumors in sites readily accessible to circulation such as BM and lungs, while intestines and secondary lymphoid sites may be less amenable to NK cell-mediated immune surveillance. This site-specific segregation of NK cell maintenance and differentiation is consistent with the preferential role of NK cells in controlling the dissemination of infected cells and tumor cell metastasis (Morvan and Lanier, 2016).

In conclusion, tissue-intrinsic modes of NK cell maintenance, differentiation, and functional regulation revealed here can drive future efforts to develop anti-tumor and anti-viral immunotherapies to leverage these distinct features of NK cell immunity.

STAR★METHODS

Detailed methods are provided in the online version of this paper and include the following:

- KEY RESOURCES TABLE
- LEAD CONTACT AND MATERIALS AVAILABILITY
- MATERIALS AVAILABILITY STATEMENT
- EXPERIMENTAL MODEL AND SUBJECT DETAILS
  - Human samples
- METHOD DETAILS
  - Isolation and preparation of single cell suspensions from tissue samples
  - Flow cytometry analysis and cell sorting
  - High-dimensional parameter flow cytometric analysis of NK cell subsets
  - *In vitro* cytokine stimulation and functional assays of NK cells
- QUANTIFICATION AND STATISTICAL ANALYSIS
  - Whole transcriptome profiling of NK cell subsets
  - Gene Set Enrichment Analysis
  - Statistical Analysis
- DATA AND CODE AVAILABILITY

SUPPLEMENTAL INFORMATION

Supplemental Information can be found online at https://doi.org/10.1016/j.cell.2020.01.022.

A video abstract is available at https://doi.org/10.1016/j.cell.2020.01.022#mmc5.

ACKNOWLEDGMENTS

This work was supported by an IOF grant from the National Institutes of Health (NIH) Human Immunology Project Consortium (HIPC) awarded to D.L.F. and L.L.L., NIH grants AI128949 and AI06697 awarded to D.L.F., and U19AI128913 to L.L.L. P.D. was supported by a Cancer Research Institute (CRI) Irvington Postdoctoral Fellowship. P.A.S was supported by an American Associate of Immunologists (AAI) Intersect Fellowship. M.T. was supported by Hungarian Campus Mundi program. D.C. was supported by T32 grant HL007854. Research reported in this publication was performed in the CCTI Flow Cytometry Core, supported in part by NIH S10RR027050. We thank our colleagues Aaron Tyznik and Bob Balderas at BD Biosciences for invaluable help in developing the NK receptor high-parameter FACS panel used in this study, Federico Gherardini at the Parker Institute for Cancer Immunotherapy for developing data analysis tools, Drs. David Artis and Laurel Monticelli for helpful discussions on ILC, and Ms. Emma Idzikowski for help with figures. The content is solely the responsibility of the authors and does not necessarily represent the official views of the NIH. We wish to gratefully acknowledge the generosity of the donor families and the exceptional efforts of Dr. Amy Friedman and LiveOnNY transplant coordinators and staff for making this study possible.

AUTHOR CONTRIBUTIONS

P.D. designed the experiments, processed tissues, performed flow cytometry, collected the data, analyzed the transcriptomics data, and wrote the paper. C.R., J.L., and J.A.-H. performed and analyzed the high-dimension flow cytometry data. P.T., P.A.S., M.T., and M.M.L.P. assisted with tissue processing. D.J.C., T.S., M.K., and R.M. obtained donor tissues. W.M. and Y.S. planned experiments and analyzed the transcriptomics data. L.F. planned the experiments and analyzed the high-dimension flow cytometry data. L.L.L. advised and consulted on all aspects of this work and provided expertise on NK cell biology. D.L.F. planned experiments, coordinated tissue acquisition and data acquisition/analysis, analyzed data, and wrote the paper.

DECLARATION OF INTERESTS

The authors declare no competing interests.

Received: June 19, 2019
Revised: October 9, 2019
Accepted: January 15, 2020
Published: February 13, 2020

REFERENCES

Abel, A.M., Yang, C., Thakar, M.S., and Malarkannan, S. (2018). Natural Killer Cells: Development, Maturation, and Clinical Utilization. Front. Immunol. *9*, 1869.

Alter, G., Malenfant, J.M., and Altfeld, M. (2004). CD107a as a functional marker for the identification of natural killer cell activity. J. Immunol. Methods *294*, 15–22.

Arase, H., Mocarski, E.S., Campbell, A.E., Hill, A.B., and Lanier, L.L. (2002). Direct recognition of cytomegalovirus by activating and inhibitory NK cell receptors. Science *296*, 1323–1326.

Aste-Amezaga, M., D'Andrea, A., Kubin, M., and Trinchieri, G. (1994). Cooperation of natural killer cell stimulatory factor/interleukin-12 with other stimuli in the induction of cytokines and cytotoxic cell-associated molecules in human T and NK cells. Cell. Immunol. *156*, 480–492.

Bengsch, B., Ohtani, T., Herati, R.S., Bovenschen, N., Chang, K.M., and Wherry, E.J. (2018). Deep immune profiling by mass cytometry links human T and NK cell differentiation and cytotoxic molecule expression patterns. J. Immunol. Methods *453*, 3–10.

Björkström, N.K., Riese, P., Heuts, F., Andersson, S., Fauriat, C., Ivarsson, M.A., Björklund, A.T., Flodström-Tullberg, M., Michaëlsson, J., Rottenberg, M.E., et al. (2010). Expression patterns of NKG2A, KIR, and CD57 define a process of CD56dim NK-cell differentiation uncoupled from NK-cell education. Blood *116*, 3853–3864.

Bottcher, J.P., Bonavita, E., Chakravarty, P., Blees, H., Cabeza-Cabrerizo, M., Sammicheli, S., Rogers, N.C., Sahai, E., Zelenay, S., and Reis e Sousa, C. (2018). NK Cells Stimulate Recruitment of cDC1 into the Tumor Microenvironment Promoting Cancer Immune Control. Cell *172*, 1022–1037.

Carpenter, D.J., Granot, T., Matsuoka, N., Senda, T., Kumar, B.V., Thome, J.J.C., Gordon, C.L., Miron, M., Weiner, J., Connors, T., et al. (2018). Human immunology studies using organ donors: Impact of clinical variations on immune parameters in tissues and circulation. Am. J. Transplant. *18*, 74–88.

Carson, W.E., Giri, J.G., Lindemann, M.J., Linett, M.L., Ahdieh, M., Paxton, R., Anderson, D., Eisenmann, J., Grabstein, K., and Caligiuri, M.A. (1994). Interleukin (IL) 15 is a novel cytokine that activates human natural killer cells via components of the IL-2 receptor. J. Exp. Med. *180*, 1395–1403.

Castriconi, R., Carrega, P., Dondero, A., Bellora, F., Casu, B., Regis, S., Ferlazzo, G., and Bottino, C. (2018). Molecular Mechanisms Directing Migration and Retention of Natural Killer Cells in Human Tissues. Front. Immunol. *9*, 2324.

Cerwenka, A., and Lanier, L.L. (2001). Natural killer cells, viruses and cancer. Nat. Rev. Immunol. *1*, 41–49.

Chen, E.Y., Tan, C.M., Kou, Y., Duan, Q., Wang, Z., Meirelles, G.V., Clark, N.R., and Ma'ayan, A. (2013). Enrichr: interactive and collaborative HTML5 gene list enrichment analysis tool. BMC Bioinformatics *14*, 128.

Collins, P.L., Cella, M., Porter, S.I., Li, S., Gurewitz, G.L., Hong, H.S., Johnson, R.P., Oltz, E.M., and Colonna, M. (2019). Gene Regulatory Programs Conferring Phenotypic Identities to Human NK Cells. Cell *176*, 348–360.

Colonna, M., Navarro, F., Bellón, T., Llano, M., García, P., Samaridis, J., Angman, L., Cella, M., and López-Botet, M. (1997). A common inhibitory receptor for major histocompatibility complex class I molecules on human lymphoid and myelomonocytic cells. J. Exp. Med. *186*, 1809–1818.

Colonna, M., Nakajima, H., Navarro, F., and López-Botet, M. (1999). A novel family of Ig-like receptors for HLA class I molecules that modulate function of lymphoid and myeloid cells. J. Leukoc. Biol. *66*, 375–381.

Cooper, M.A., Fehniger, T.A., Turner, S.C., Chen, K.S., Ghaheri, B.A., Ghayur, T., Carson, W.E., and Caligiuri, M.A. (2001). Human natural killer cells: a unique innate immunoregulatory role for the CD56(bright) subset. Blood *97*, 3146–3151.

Cooper, M.A., Elliott, J.M., Keyel, P.A., Yang, L., Carrero, J.A., and Yokoyama, W.M. (2009). Cytokine-induced memory-like natural killer cells. Proc. Natl. Acad. Sci. USA *106*, 1915–1919.

Crinier, A., Milpied, P., Escaliere, B., Piperoglou, C., Galluso, J., Balsamo, A., Spinelli, L., Cervera-Marzal, I., Ebbo, M., Girard-Madoux, M., et al. (2018). High-Dimensional Single-Cell Analysis Identifies Organ-Specific Signatures and Conserved NK Cell Subsets in Humans and Mice. Immunity *49*, 971–986.

Daniels, K.A., Devora, G., Lai, W.C., O'Donnell, C.L., Bennett, M., and Welsh, R.M. (2001). Murine cytomegalovirus is regulated by a discrete subset of natural killer cells reactive with monoclonal antibody to Ly49H. J. Exp. Med. *194*, 29–44.

Di Santo, J.P., and Vosshenrich, C.A. (2006). Bone marrow versus thymic pathways of natural killer cell development. Immunol. Rev. *214*, 35–46.

Dobin, A., Davis, C.A., Schlesinger, F., Drenkow, J., Zaleski, C., Jha, S., Batut, P., Chaisson, M., and Gingeras, T.R. (2013). STAR: ultrafast universal RNA-seq aligner. Bioinformatics *29*, 15–21.

Dokun, A.O., Kim, S., Smith, H.R., Kang, H.S., Chu, D.T., and Yokoyama, W.M. (2001). Specific and nonspecific NK cell activation during virus infection. Nat. Immunol. *2*, 951–956.

Faridi, R.M., and Agrawal, S. (2011). Killer immunoglobulin-like receptors (KIRs) and HLA-C allorecognition patterns implicative of dominant activation of natural killer cells contribute to recurrent miscarriages. Hum. Reprod. *26*, 491–497.

Fehniger, T.A., Shah, M.H., Turner, M.J., VanDeusen, J.B., Whitman, S.P., Cooper, M.A., Suzuki, K., Wechser, M., Goodsaid, F., and Caligiuri, M.A. (1999). Differential cytokine and chemokine gene expression by human NK cells following activation with IL-18 or IL-15 in combination with IL-12: implications for the innate immune response. J. Immunol. *162*, 4511–4520.

Fehniger, T.A., Cai, S.F., Cao, X., Bredemeyer, A.J., Presti, R.M., French, A.R., and Ley, T.J. (2007). Acquisition of murine NK cell cytotoxicity requires the translation of a pre-existing pool of granzyme B and perforin mRNAs. Immunity *26*, 798–811.

Freud, A.G., Becknell, B., Roychowdhury, S., Mao, H.C., Ferketich, A.K., Nuovo, G.J., Hughes, T.L., Marburger, T.B., Sung, J., Baiocchi, R.A., et al. (2005). A human CD34(+) subset resides in lymph nodes and differentiates into CD56bright natural killer cells. Immunity *22*, 295–304.

Freud, A.G., Mundy-Bosse, B.L., Yu, J., and Caligiuri, M.A. (2017). The Broad Spectrum of Human Natural Killer Cell Diversity. Immunity *47*, 820–833.

Gaynor, L.M., and Colucci, F. (2017). Uterine Natural Killer Cells: Functional Distinctions and Influence on Pregnancy in Humans and Mice. Front. Immunol. *8*, 467.

Gebhardt, T., Palendira, U., Tscharke, D.C., and Bedoui, S. (2018). Tissue-resident memory T cells in tissue homeostasis, persistent infection, and cancer surveillance. Immunol. Rev. *283*, 54–76.

Geissmann, F., Cameron, T.O., Sidobre, S., Manlongat, N., Kronenberg, M., Briskin, M.J., Dustin, M.L., and Littman, D.R. (2005). Intravascular immune surveillance by CXCR6+ NKT cells patrolling liver sinusoids. PLoS Biol. *3*, e113.

Gordon, C.L., Miron, M., Thome, J.J., Matsuoka, N., Weiner, J., Rak, M.A., Igarashi, S., Granot, T., Lerner, H., Goodrum, F., and Farber, D.L. (2017). Tissue reservoirs of antiviral T cell immunity in persistent human CMV infection. J. Exp. Med. *214*, 651–667.

Granot, T., Senda, T., Carpenter, D.J., Matsuoka, N., Weiner, J., Gordon, C.L., Miron, M., Kumar, B.V., Griesemer, A., Ho, S.H., et al. (2017). Dendritic Cells Display Subset and Tissue-Specific Maturation Dynamics over Human Life. Immunity *46*, 504–515.

Gumá, M., Angulo, A., Vilches, C., Gómez-Lozano, N., Malats, N., and López-Botet, M. (2004). Imprint of human cytomegalovirus infection on the NK cell receptor repertoire. Blood *104*, 3664–3671.

Gumá, M., Budt, M., Sáez, A., Brckalo, T., Hengel, H., Angulo, A., and López-Botet, M. (2006). Expansion of CD94/NKG2C+ NK cells in response to human cytomegalovirus-infected fibroblasts. Blood *107*, 3624–3631.

Hendricks, D.W., Balfour, H.H., Jr., Dunmire, S.K., Schmeling, D.O., Hogquist, K.A., and Lanier, L.L. (2014). Cutting edge: NKG2C(hi)CD57+ NK cells respond specifically to acute infection with cytomegalovirus and not Epstein-Barr virus. J. Immunol. *192*, 4492–4496.

Hibbs, M.L., Selvaraj, P., Carpén, O., Springer, T.A., Kuster, H., Jouvin, M.H., and Kinet, J.P. (1989). Mechanisms for regulating expression of membrane isoforms of Fc gamma RIII (CD16). Science *246*, 1608–1611.

Hombrink, P., Helbig, C., Backer, R.A., Piet, B., Oja, A.E., Stark, R., Brasser, G., Jongejan, A., Jonkers, R.E., Nota, B., et al. (2016). Programs for the persistence, vigilance and control of human CD8^{+} lung-resident memory T cells. Nat. Immunol. *17*, 1467–1478.

Horowitz, A., Strauss-Albee, D.M., Leipold, M., Kubo, J., Nemat-Gorgani, N., Dogan, O.C., Dekker, C.L., Mackey, S., Maecker, H., Swan, G.E., et al. (2013). Genetic and environmental determinants of human NK cell diversity revealed by mass cytometry. Sci. Transl. Med. *5*, 208ra145.

Hudspeth, K., Donadon, M., Cimino, M., Pontarini, E., Tentorio, P., Preti, M., Hong, M., Bertoletti, A., Bicciato, S., Invernizzi, P., et al. (2016). Human liver-resident CD56(bright)/CD16(neg) NK cells are retained within hepatic sinusoids via the engagement of CCR5 and CXCR6 pathways. J. Autoimmun. *66*, 40–50.

Hunter, J.D. (2007). Matplotlib: A 2D graphics environment. Comput. Sci. Eng. *9*, 90–95.

Imai, K., Matsuyama, S., Miyake, S., Suga, K., and Nakachi, K. (2000). Natural cytotoxic activity of peripheral-blood lymphocytes and cancer incidence: an 11-year follow-up study of a general population. Lancet *356*, 1795–1799.

Jiang, X., Clark, R.A., Liu, L., Wagers, A.J., Fuhlbrigge, R.C., and Kupper, T.S. (2012). Skin infection generates non-migratory memory CD8+ T(RM) cells providing global skin immunity. Nature *483*, 227–231.

Jones, E., Oliphant, T., and Peterson, P. (2001). SciPy: Open source scientific tools for Python. http://www.scipy.org/.

Kelly, J.M., Darcy, P.K., Markby, J.L., Godfrey, D.I., Takeda, K., Yagita, H., and Smyth, M.J. (2002). Induction of tumor-specific T cell memory by NK cell-mediated tumor rejection. Nat. Immunol. *3*, 83–90.

Kolde, R. (2012). Pheatmap: pretty heatmaps. R Package Version.. https://CRAN.R-project.org/package=pheatmap

Koopman, L.A., Kopcow, H.D., Rybalov, B., Boyson, J.E., Orange, J.S., Schatz, F., Masch, R., Lockwood, C.J., Schachter, A.D., Park, P.J., and Strominger, J.L. (2003). Human decidual natural killer cells are a unique NK cell subset with immunomodulatory potential. J. Exp. Med. *198*, 1201–1212.

Kumar, B.V., Ma, W., Miron, M., Granot, T., Guyer, R.S., Carpenter, D.J., Senda, T., Sun, X., Ho, S.H., Lerner, H., et al. (2017). Human Tissue-Resident Memory T Cells Are Defined by Core Transcriptional and Functional Signatures in Lymphoid and Mucosal Sites. Cell Rep. *20*, 2921–2934.

Kuo, C.T., and Leiden, J.M. (1999). Transcriptional regulation of T lymphocyte development and function. Annu. Rev. Immunol. *17*, 149–187.

Lanier, L.L. (2008). Up on the tightrope: natural killer cell activation and inhibition. Nat. Immunol. *9*, 495–502.

Lanier, L.L., Le, A.M., Civin, C.I., Loken, M.R., and Phillips, J.H. (1986). The relationship of CD16 (Leu-11) and Leu-19 (NKH-1) antigen expression on human peripheral blood NK cells and cytotoxic T lymphocytes. J. Immunol. *136*, 4480–4486.

Lanier, L.L., Yu, G., and Phillips, J.H. (1989). Co-association of CD3 zeta with a receptor (CD16) for IgG Fc on human natural killer cells. Nature *342*, 803–805.

Lee, J., Zhang, T., Hwang, I., Kim, A., Nitschke, L., Kim, M., Scott, J.M., Kamimura, Y., Lanier, L.L., and Kim, S. (2015). Epigenetic modification and antibody-dependent expansion of memory-like NK cells in human cytomegalovirus-infected individuals. Immunity *42*, 431–442.

Leek, J.T., Johnson, W.E., Parker, H.S., Fertig, E.J., Jaffe, A.E., Storey, J.D., Zhang, Y., and Torres, L.C. (2019). sva: Surrogate Variable Analysis. R package version 3321, https://bioconductor.org/packages/release/bioc/html/sva.html.

Li, N., van Unen, V., Höllt, T., Thompson, A., van Bergen, J., Pezzotti, N., Eisemann, E., Vilanova, A., Chuva de Sousa Lopes, S.M., Lelieveldt, B.P.F., and Koning, F. (2018). Mass cytometry reveals innate lymphoid cell differentiation pathways in the human fetal intestine. J. Exp. Med. *215*, 1383–1396.

Lopez-Vergès, S., Milush, J.M., Pandey, S., York, V.A., Arakawa-Hoyt, J., Pircher, H., Norris, P.J., Nixon, D.F., and Lanier, L.L. (2010). CD57 defines a functionally distinct population of mature NK cells in the human CD56dimCD16+ NK-cell subset. Blood *116*, 3865–3874.

Lopez-Vergès, S., Milush, J.M., Schwartz, B.S., Pando, M.J., Jarjoura, J., York, V.A., Houchins, J.P., Miller, S., Kang, S.-M., Norris, P.J., et al. (2011). Expansion of a unique CD57^{+}NKG2Chi natural killer cell subset during acute human cytomegalovirus infection. Proc. Natl. Acad. Sci. USA *108*, 14725–14732.

Love, M.I., Huber, W., and Anders, S. (2014). Moderated estimation of fold change and dispersion for RNA-seq data with DESeq2. Genome Biol. *15*, 550.

Luther, C., Warner, K., and Takei, F. (2011). Unique progenitors in mouse lymph node develop into CD127+ NK cells: thymus-dependent and thymus-independent pathways. Blood *117*, 4012–4021.

Mackay, L.K., Minnich, M., Kragten, N.A., Liao, Y., Nota, B., Seillet, C., Zaid, A., Man, K., Preston, S., Freestone, D., et al. (2016). Hobit and Blimp1 instruct a universal transcriptional program of tissue residency in lymphocytes. Science *352*, 459–463.

Marini, F., and Binder, H. (2019). pcaExplorer: an R/Bioconductor package for interacting with RNA-seq principal components. BMC Bioinformatics *20*, 331.

Marquardt, N., Kekalainen, E., Chen, P., Kvedaraite, E., Wilson, J.N., Ivarsson, M.A., Mjosberg, J., Berglin, L., Safholm, J., Manson, M.L., et al. (2017). Human lung natural killer cells are predominantly comprised of highly differentiated hypofunctional CD69(-)CD56(dim) cells. J. Allergy Clin. Immunol. *139*, 1321–1330.

Marquardt, N., Kekäläinen, E., Chen, P., Lourda, M., Wilson, J.N., Scharenberg, M., Bergman, P., Al-Ameri, M., Hård, J., Mold, J.E., et al. (2019). Unique transcriptional and protein-expression signature in human lung tissue-resident NK cells. Nat. Commun. *10*, 3841.

Masopust, D., and Soerens, A.G. (2019). Tissue-Resident T Cells and Other Resident Leukocytes. Annu. Rev. Immunol. *37*, 521–546.

Melsen, J.E., Lugthart, G., Vervat, C., Kielbasa, S.M., van der Zeeuw, S.A.J., Buermans, H.P.J., van Ostaijen-Ten Dam, M.M., Lankester, A.C., and Schilham, M.W. (2018). Human Bone Marrow-Resident Natural Killer Cells Have a Unique Transcriptional Profile and Resemble Resident Memory CD8^{+} T Cells. Front. Immunol. *9*, 1829.

Miron, M., Kumar, B.V., Meng, W., Granot, T., Carpenter, D.J., Senda, T., Chen, D., Rosenfeld, A.M., Zhang, B., Lerner, H., et al. (2018). Human Lymph Nodes Maintain TCF-1^{hi} Memory T Cells with High Functional Potential and Clonal Diversity throughout Life. J. Immunol. *201*, 2132–2140.

Montaldo, E., Vacca, P., Chiossone, L., Croxatto, D., Loiacono, F., Martini, S., Ferrero, S., Walzer, T., Moretta, L., and Mingari, M.C. (2016). Unique Eomes(+) NK Cell Subsets Are Present in Uterus and Decidua During Early Pregnancy. Front. Immunol. *6*, 646.

Morvan, M.G., and Lanier, L.L. (2016). NK cells and cancer: you can teach innate cells new tricks. Nat. Rev. Cancer *16*, 7–19.

Muruganandah, V., Sathkumara, H.D., Navarro, S., and Kupz, A. (2018). A Systematic Review: The Role of Resident Memory T Cells in Infectious Diseases and Their Relevance for Vaccine Development. Front. Immunol. *9*, 1574.

Nagler, A., Lanier, L.L., Cwirla, S., and Phillips, J.H. (1989). Comparative studies of human FcRIII-positive and negative natural killer cells. J. Immunol. *143*, 3183–3191.

Nikolich-Žugich, J. (2018). The twilight of immunity: emerging concepts in aging of the immune system. Nat. Immunol. *19*, 10–19.

O'Leary, J.G., Goodarzi, M., Drayton, D.L., and von Andrian, U.H. (2006). T cell- and B cell-independent adaptive immunity mediated by natural killer cells. Nat. Immunol. *7*, 507–516.

O'Sullivan, T.E., Sun, J.C., and Lanier, L.L. (2015). Natural Killer Cell Memory. Immunity *43*, 634–645.

Orange, J.S. (2006). Human natural killer cell deficiencies. Curr. Opin. Allergy Clin. Immunol. *6*, 399–409.

Pawelec, G., and Derhovanessian, E. (2011). Role of CMV in immune senescence. Virus Res. *157*, 175–179.

Pegram, H.J., Andrews, D.M., Smyth, M.J., Darcy, P.K., and Kershaw, M.H. (2011). Activating and inhibitory receptors of natural killer cells. Immunol. Cell Biol. *89*, 216–224.

Peng, H., and Tian, Z. (2017). Diversity of tissue-resident NK cells. Semin. Immunol. *31*, 3–10.

Poggi, A., Benelli, R., Venè, R., Costa, D., Ferrari, N., Tosetti, F., and Zocchi, M.R. (2019). Human Gut-Associated Natural Killer Cells in Health and Disease. Front. Immunol. *10*, 961.

Qiu, P., Simonds, E.F., Bendall, S.C., Gibbs, K.D., Jr., Bruggner, R.V., Linderman, M.D., Sachs, K., Nolan, G.P., and Plevritis, S.K. (2011). Extracting a cellular hierarchy from high-dimensional cytometry data with SPADE. Nat. Biotechnol. *29*, 886–891.

Robertson, M.J., and Ritz, J. (1990). Biology and clinical relevance of human natural killer cells. Blood *76*, 2421–2438.

Scalzo, A.A., Corbett, A.J., Rawlinson, W.D., Scott, G.M., and Degli-Esposti, M.A. (2007). The interplay between host and viral factors in shaping the outcome of cytomegalovirus infection. Immunol. Cell Biol. *85*, 46–54.

Schenkel, J.M., Fraser, K.A., and Masopust, D. (2014). Cutting edge: resident memory CD8 T cells occupy frontline niches in secondary lymphoid organs. J. Immunol. *192*, 2961–2964.

Schlums, H., Cichocki, F., Tesi, B., Theorell, J., Beziat, V., Holmes, T.D., Han, H., Chiang, S.C., Foley, B., Mattsson, K., et al. (2015). Cytomegalovirus infection drives adaptive epigenetic diversification of NK cells with altered signaling and effector function. Immunity *42*, 443–456.

Scoville, S.D., Freud, A.G., and Caligiuri, M.A. (2017). Modeling Human Natural Killer Cell Development in the Era of Innate Lymphoid Cells. Front. Immunol. *8*, 360.

Senda, T., Dogra, P., Granot, T., Furuhashi, K., Snyder, M.E., Carpenter, D.J., Szabo, P.A., Thapa, P., Miron, M., and Farber, D.L. (2019). Microanatomical dissection of human intestinal T-cell immunity reveals site-specific changes in gut-associated lymphoid tissues over life. Mucosal Immunol. *12*, 378–389.

Shi, F.D., Ljunggren, H.G., La Cava, A., and Van Kaer, L. (2011). Organ-specific features of natural killer cells. Nat. Rev. Immunol. *11*, 658–671.

Sojka, D.K., Plougastel-Douglas, B., Yang, L., Pak-Wittel, M.A., Artyomov, M.N., Ivanova, Y., Zhong, C., Chase, J.M., Rothman, P.B., Yu, J., et al. (2014). Tissue-resident natural killer (NK) cells are cell lineages distinct from thymic and conventional splenic NK cells. eLife *3*, e01659.

Sun, J.C., Beilke, J.N., and Lanier, L.L. (2009). Adaptive immune features of natural killer cells. Nature *457*, 557–561.

Sun, J.C., Beilke, J.N., and Lanier, L.L. (2010). Immune memory redefined: characterizing the longevity of natural killer cells. Immunol. Rev. *236*, 83–94.

Sun, J.C., Madera, S., Bezman, N.A., Beilke, J.N., Kaplan, M.H., and Lanier, L.L. (2012). Proinflammatory cytokine signaling required for the generation of natural killer cell memory. J. Exp. Med. *209*, 947–954.

Szabo, P.A., Miron, M., and Farber, D.L. (2019). Location, location, location: Tissue resident memory T cells in mice and humans. Sci. Immunol. *4*, eaas9673.

Teijaro, J.R., Turner, D., Pham, Q., Wherry, E.J., Lefrançois, L., and Farber, D.L. (2011). Cutting edge: Tissue-retentive lung memory CD4 T cells mediate optimal protection to respiratory virus infection. J. Immunol. *187*, 5510–5514.

Thome, J.J., Yudanin, N., Ohmura, Y., Kubota, M., Grinshpun, B., Sathaliyawala, T., Kato, T., Lerner, H., Shen, Y., and Farber, D.L. (2014). Spatial map of human T cell compartmentalization and maintenance over decades of life. Cell *159*, 814–828.

Victorino, F., Sojka, D.K., Brodsky, K.S., McNamee, E.N., Masterson, J.C., Homann, D., Yokoyama, W.M., Eltzschig, H.K., and Clambey, E.T. (2015). Tissue-Resident NK Cells Mediate Ischemic Kidney Injury and Are Not Depleted by Anti-Asialo-GM1 Antibody. J. Immunol. *195*, 4973–4985.

Vivier, E., Ugolini, S., Blaise, D., Chabannon, C., and Brossay, L. (2012). Targeting natural killer cells and natural killer T cells in cancer. Nat. Rev. Immunol. *12*, 239–252.

Vivier, E., Artis, D., Colonna, M., Diefenbach, A., Di Santo, J.P., Eberl, G., Koyasu, S., Locksley, R.M., McKenzie, A.N.J., Mebius, R.E., et al. (2018). Innate Lymphoid Cells: 10 Years On. Cell *174*, 1054–1066.

Vosshenrich, C.A., García-Ojeda, M.E., Samson-Villéger, S.I., Pasqualetto, V., Enault, L., Richard-Le Goff, O., Corcuff, E., Guy-Grand, D., Rocha, B., Cumano, A., et al. (2006). A thymic pathway of mouse natural killer cell development characterized by expression of GATA-3 and CD127. Nat. Immunol. *7*, 1217–1224.

Wang, W., Erbe, A.K., Hank, J.A., Morris, Z.S., and Sondel, P.M. (2015). NK Cell-Mediated Antibody-Dependent Cellular Cytotoxicity in Cancer Immunotherapy. Front. Immunol. *6*, 368.

Wang, J., Vasaikar, S., Shi, Z., Greer, M., and Zhang, B. (2017). WebGestalt 2017: a more comprehensive, powerful, flexible and interactive gene set enrichment analysis toolkit. Nucleic Acids Res. *45* (W1), W130–W137.

Wickham, H. (2016). ggplot2: Elegant Graphics for Data Analysis (Springer-Verlag).

Yu, J., Freud, A.G., and Caligiuri, M.A. (2013). Location and cellular stages of natural killer cell development. Trends Immunol. *34*, 573–582.

Yudanin, N.A., Schmitz, F., Flamar, A.L., Thome, J.J.C., Tait Wojno, E., Moeller, J.B., Schirmer, M., Latorre, I.J., Xavier, R.J., Farber, D.L., et al. (2019). Spatial and Temporal Mapping of Human Innate Lymphoid Cells Reveals Elements of Tissue Specificity. Immunity *50*, 505–519.

Zhang, T., Scott, J.M., Hwang, I., and Kim, S. (2013). Cutting edge: antibody-dependent memory-like NK cells distinguished by FcRγ deficiency. J. Immunol. *190*, 1402–1406.

Zhou, X., Yu, S., Zhao, D.M., Harty, J.T., Badovinac, V.P., and Xue, H.H. (2010). Differentiation and persistence of memory CD8(+) T cells depend on T cell factor 1. Immunity *33*, 229–240.

Zwirner, N.W., and Ziblat, A. (2017). Regulation of NK Cell Activation and Effector Functions by the IL-12 Family of Cytokines: The Case of IL-27. Front. Immunol. *8*, 25.

STAR★METHODS

KEY RESOURCES TABLE

REAGENT or RESOURCE	SOURCE	IDENTIFIER
Conventional flow cytometry		
Anti-Human CD45 AF700	BioLegend	RRID: AB_493761
Anti-Human CD45 BV510	BioLegend	RRID: AB_2561940
Anti-Human CD14 BUV737	BD-Biosciences	RRID: AB_2744285
Anti-Human CD19 BUV737	BD-Biosciences	Cat# 564304
Anti-Human CD3 BV650	BioLegend	RRID: AB_2563352
Anti-Human CD56 PE-Cy7	BioLegend	RRID: AB_2563927
Anti-Human CD56 APC-Vio770	Miltenyi Biotec	Cat# 130-100-690
Anti-Human CD16 BV605	BioLegend	RRID: AB_2562990
Anti-Human CD57 PE Dazzle	BioLegend	RRID: AB_2564063
Anti-Human CD159c NKG2C PE	R&D System	Cat# FAB138P-100
Anti-Human FcεR1γ FITC	Millipore	RRID: AB_11203492
Anti-Human GzmB AF700	BD-Biosciences	RRID: AB_1645453
Anti-Human Ifng BB700	BD-Biosciences	RRID: AB_2744484
Anti-Human CD107a BUV395	BD-Biosciences	RRID: AB_2739073
Anti-Human CD69 BV711	BioLegend	RRID: AB_2566466
Anti-Human CD103 BUV395	BD-Biosciences	RRID: AB_2738759
Anti-Human CXCR6 BV510	BD-Biosciences	RRID: AB_2741610
Anti-Human CD49a BV786	BD-Biosciences	RRID: AB_2740720
Anti-Human Tbet BV421	BioLegend	RRID: AB_10896427
Anti-Human TCF1 PE	Cell Signaling Technologies	RRID: AB_2798483
Anti-Human CD127 BV421	BioLegend	RRID: AB_10960140
Anti-Human RORγt AF647	BD-Biosciences	RRID: AB_2738324
High-dimensional flow cytometry		
Anti-Human CD160 AF488	BD Bioscience	RRID: AB_11153688
Anti-Human CD27 BB660	BD Bioscience	Clone:M-T271
Anti-Human CD28 BB700	BD Bioscience	Clone:CD28.2
Anti-Human CD161 BB790	BD Bioscience	Clone:DX12
Anti-Human CD159c NKG2C PE	R&D System	Cat# FAB138P-100
Anti-Human CD56 PE-CF594	BD Bioscience	RRID: AB_2738983
Anti-Human CD85J PE-Cy5	BD Bioscience	RRID: AB_394021
Anti-Human CD159a NKG2A PE-Vio770	Miltenyi	RRID: AB_2726172
Anti-Human CD158b KIRsDL2/3 APC	Miltenyi	RRID: AB_871609
Anti-Human CD158b KIR2DL1/DS1,3,5 APC	BioLegend	RRID: AB_2565577
Anti-Human CD158e KIR3DL1 APC	BD Bioscience	Clone:DX9
Anti-Human CD45 AF700	BioLegend	RRID: AB_2566374
Anti-Human CD3 APC-H7	BD Bioscience	RRID: AB_1645476
Anti-Human TCRγδ BV421	BD Bioscience	RRID: AB_2737655
Anti-Human CD294 BV480	BD Bioscience	RRID: AB_2743703
Anti-Human TCRVd2 BV605	BD Bioscience	RRID: AB_2741719
Anti-Human CD137 (4-1BB) BV650	BD Bioscience	RRID: AB_2738586
Anti-Human CD314 NKG2D BV711	BD Bioscience	RRID: AB_2738377
Anti-Human CD127 BV750	BD Bioscience	Clone:HIL-7R-M21
Anti-Human CD336 NKp44 BV786	BD Bioscience	RRID: AB_2742134
Anti-Human CD8 BUV395	BD Bioscience	RRID: AB_2722501

(*Continued on next page*)

Continued

REAGENT or RESOURCE	SOURCE	IDENTIFIER
Anti-Human CD14 BUV496	BD Bioscience	Clone:M5E2
Anti-Human CD19 BUV496	BD Bioscience	RRID: AB_2744311
Anti-Human CD337 NKp30 BUV563	BD Bioscience	Clone:P30-15
Anti-Human CD57 BUV615	BD Bioscience	Clone:NK1
Anti-Human CD335 NKp46 BUV661	BD Bioscience	Clone:9E2/Nkp46
Anti-Human CD279 PD-1 BUV737	BD Bioscience	RRID: AB_2739167
Anti-Human CD16 BUV805	BD Bioscience	Clone:3G8
Cell sorting		
Anti-Human CD45 BV510	BioLegend	RRID: AB_2561940
Anti-Human CD14 APC	BioLegend	RRID: AB_830681
Anti-Human CD19 APC	Tonbo	Cat#20-0199-T100
Anti-Human CD3 FITC	BioLegend	RRID: AB_571907
Anti-Human CD56 PE-Cy7	BioLegend	RRID: AB_2563927
Chemicals, Peptides, and Recombinant Proteins		
Recombinant Human IL-12	PeproTech	Cat#200-12
Recombinant Human IL-15	PeproTech	Cat#200-15
Recombinant Human IL-18	MBL International Corp.	Cat#B001-5
Human TrueStain FcX	BioLegend	Cat#422302
Fixable Viability Dye eFluor 780	eBioscience	Cat#65-0865-14
Live/Dead BV570	BD Bioscience	Cat#FVS575V
RPMI 1640	Corning	Cat#10-040-CM
Deposited Data		
Raw and analyzed data	This paper	GEO: GSE133383
Experimental Models: Cell Lines		
K652 cell line	ATCC	Cat#ATCC CCL-243
Software and Algorithms		
STARaligner	https://github.com/alexdobin/STAR	Dobin et al., 2013
DEseq2	N/A	Love et al., 2014
Enrichr	https://amp.pharm.mssm.edu/Enrichr/	Chen et al., 2013
WebGestalt	http://www.webgestalt.org/	Wang et al., 2017
Rstudio version 1.2.1335	RStudio, Inc. (2019)	https://rstudio.com
R version 3.5	R Foundation for StatisticalComputing (2017)	https://www.R-project.org
Other		
EasySep Human NK Cell Enrichment Kit	Stem Cell Tech	Cat#19055

LEAD CONTACT AND MATERIALS AVAILABILITY

Further information and requests for reagents should be directed to and will be fulfilled by lead author Donna L. Farber (df2396@cumc.columbia.edu)

MATERIALS AVAILABILITY STATEMENT

This study did not generate new unique reagents.

EXPERIMENTAL MODEL AND SUBJECT DETAILS

Human samples

Tissues were obtained from deceased organ donors as part of organ acquisition for clinical transplantation through an approved protocol and material transfer agreement with LiveOnNY as described previously (Carpenter et al., 2018; Gordon et al., 2017; Granot

et al., 2017; Kumar et al., 2017; Miron et al., 2018; Senda et al., 2019). Donors were free of cancer, chronic diseases, seronegative for hepatitis B, C, and HIV, and represented diverse ages (Table S1). This study does not qualify as "human subjects" research, as confirmed by the Columbia University IRB as tissue samples were obtained from brain-dead (deceased) individuals.

METHOD DETAILS

Isolation and preparation of single cell suspensions from tissue samples

Tissue samples were maintained in cold saline or CoStorSol® (University of Wisconsin (UW) solution (Preservation Solutions, Elkhorn, WI, Cat# PS004)), and transported to the laboratory within 2-4 hours of organ procurement. Lymphocytes were isolated from blood and BM samples by density centrifugation using lymphocyte separation medium (Corning cat# 25-072-CI) for recovery of mononuclear cells. Spleen, lung, intestinal, tonsil, and LN samples were processed using enzymatic and mechanical digestion, resulting in high yields of live leukocytes, as previously described (Carpenter et al., 2018; Gordon et al., 2017; Granot et al., 2017; Kumar et al., 2017; Miron et al., 2018; Senda et al., 2019).

Flow cytometry analysis and cell sorting

For flow cytometric analysis, cells were stained in 96-well U-bottom plates in the dark using antibody panels (see Key Resources Table). Surface staining was done for 20min at room temperature (RT). For intracellular staining, surface stained cells were fixed for 25min at RT in fixing buffer (Invitrogen cat# 00-5123-43), followed by staining in permeabilization buffer (Invitrogen cat# 00-8333-56) at RT for 30 min. Controls were isotype stained and single-fluorochrome stained samples. Flow cytometry data were acquired on a BD LSRII and analyzed using FCS express 6 (*De Novo* Software) and custom Python scripts. Spanning-tree progression analysis of density-normalized events (SPADE) analysis of the NK cell data collected from blood, BM, spleen, lung, gut, LLN, and MLN was done using MATLAB with no down-sampling and number of clusters set to 150-200 (Qiu et al., 2011).

NK cells were purified from blood, BM, spleen, lung, and LN using EasySep Human NK Cell Enrichment Kit (Stem Cell Tech cat# 19055), followed by sorting. Enriched cells were stained with the antibody panel described in the Key Resources Table. The stained cells were sorted using a BD Influx Cell Sorter. Sorted cells were used either for functional assays or RNA isolation.

High-dimensional parameter flow cytometric analysis of NK cell subsets

For high parameter analysis using the BD Symphony panels, $5x10^6$ cells from each site were stained in 96 well v-bottom plates using an optimized antibody panel as described in the Key Resources Table. Briefly, cells were washed with PBS, re-suspended in 1 mL of viability dye and incubated at RT in the dark for 10 min. Cells were washed once with cold FACS-buffer (PBS with 2% heat-inactivated FCS and 2 mM EDTA) and stained in a two-step process. First, the cells were resuspended in a staining cocktail that included the anti-$\gamma\delta$ TCR antibody (Key Resources Table), human TrueStain FcX (BioLegend, cat: 422302), and mouse serum (Jackson Immuno Research Labs, cat: 015-000-001) and incubated on ice for 10 min. Second, following incubation, antibodies in the Key Resources Table were added together with 50 μL of Horizon Brilliant Stain buffer (BD Bioscience, cat: 56379), incubated for 25 min on ice, washed with FACS-buffer, and fixed in 100 μL of Fluorofix Buffer (BioLegend, cat# 422101). Samples were analyzed on the LSR Fortessa X50 ("Symphony") cytometer (BD Bioscience). Data were analyzed with FlowJo 10.2. NK cell populations (defined as live, $CD45^+CD14^-CD19^-CD3^-CD56^+$ lymphocytes) were exported and high-dimensional analyses were performed using the R-based workflow publicly available at https://github.com/ParkerICI/flow-analysis-tutorial and https://github.com/ParkerICI.

In vitro cytokine stimulation and functional assays of NK cells

NK cells ($CD45^+CD56^+CD3^-$) sorted from freshly processed tissue sites (see above) were cultured in 96-well u-bottom plates in RPMI-1640 medium containing fetal bovine serum (10%) with or without 10ng/ml IL-12 (PeproTech, cat# 200-12), 100ng/ml IL-15 (PeproTech, cat# 200-15) and 100ng/ml IL-18 (MBL International Corp. cat# B001-5) for 18 hours. Vesicular transport was inhibited by GolgiStop (BD Biosciences, cat# 554724) and GolgiPlug (BD Bioscience cat# 555029) during the last 6 hours of the incubation. Cell surface and intracellular staining was performed as described above.

For measuring degranulation by NK cells, 30,000-50,000 sorted, overnight rested NK cells were incubated with K562 cells (ATCC: CCL-243; provided by Emily Mace, Columbia University) at a 2:1 effector to target (NK: K562) ratio in a 96-well tissue culture plate at 37°C at 5% CO_2 for 4 hours. Anti-CD107a antibody was added to the co-culture at the beginning of the assay. Following incubation, the cells were washed once with FACS-buffer before acquiring the data. Data were acquired on a BD LSRII and analyzed using FCS express 6 (*De Novo* Software).

QUANTIFICATION AND STATISTICAL ANALYSIS

Whole transcriptome profiling of NK cell subsets

RNA was isolated from sorted $CD56^{bright}CD16^-$ and $CD56^{dim}CD16^+$ NK cells using the RNA Easy kit (QIAGEN cat # 74004) and library preparation was done using the SMART-Seq® ultra- low input RNA kit (Takara bio). Samples were sequenced at Genewiz (South Plainfield, NJ) using a HiSeq2500 system (Illumina). Trimmed paired-end reads were mapped to the *Homo sapiens* GRCh38 reference genome available on ENSEMBL using the STAR aligner v.2.5.2b. The gene list was filtered to exclude any

non-coding genes, following which genes with read counts below 5 copies in at least 9 of 30 samples were excluded from the analysis. Sequencing batch differences were removed using *sva* package (Leek et al., 2019) and differential expression (DE) gene analysis was done using the *DESeq2* (Love et al., 2014) package in R. Genes were considered as significantly differentially expressed if absolute log2fold change was ≥ 1 and p value was below the 0.05 threshold. Heatmaps were generated using the *pheatmap* (Kolde, 2012) package, and PCA plots and log2 fold change bi-plots were generated by use of the *ggplot2* package (Wickham, 2016). Clustering groups within PCA was predicted by pcaplot function of the *pcaExplorer* library (Marini and Binder, 2019). The hit counts table for the ILC study (GEO: GSE126107) (Yudanin et al., 2019) was downloaded and used to compare the transcriptional profile of ILC subsets to $CD56^{bright}CD16^{-}$ NK cell subsets from this study.

Gene Set Enrichment Analysis

For gene set enrichment analysis (GSEA) of unique tissue-specific transcriptional programs, differentially expressed genes with value of log_2-fold change ≥ 1 for comparison between tissue $CD56^{bright}CD16^{-}$ and $CD56^{dim}CD16^{+}$ NK cells, and their blood counterparts were used as input to run pre-ranked GSEA using *WebGestalt* web application (Wang et al., 2017). To test for enrichment of tissue-residence gene signature, genes ranked by absolute value of log_2-fold change between $CD56^{bright}CD16^{-}$ and $CD56^{dim}CD16^{+}$ NK cells was used as input to run pre-ranked GSEA using the Broad Institute GSEA Java web application. Gene sets were created from lung and spleen $CD8^{+}$Trm transcription profiles, as previously determined (Kumar et al., 2017).

Statistical Analysis

Graphs were generated using the Python *matplotlib* library (Hunter, 2007). To compare expression of surface and intracellular markers across different tissue sites, a one-way ANOVA test was run followed by Tukey's correction to correct for multiple testing. For comparing expression of markers between 2 groups within a tissue site we performed either a paired t test, or multiple comparison t tests with unequal variance. Nonparametric Mann-Whitney U test was used where data showed deviation from normal distribution as indicated in figure legends. *P*-values below 0.05 were considered as statistically significant. The statistical analysis was run using custom scripts based on Python *SciPy* library (Jones et al., 2001) and Prizm (GraphPad). For all figures $^{***}p \leq 0.001$, $^{**}p \leq 0.01$, and $^{*}p \leq 0.05$.

DATA AND CODE AVAILABILITY

The processed data and transcriptome dataset generated during this study is available on NCBI GEO with the accession number GEO: GSE133383.

Cell

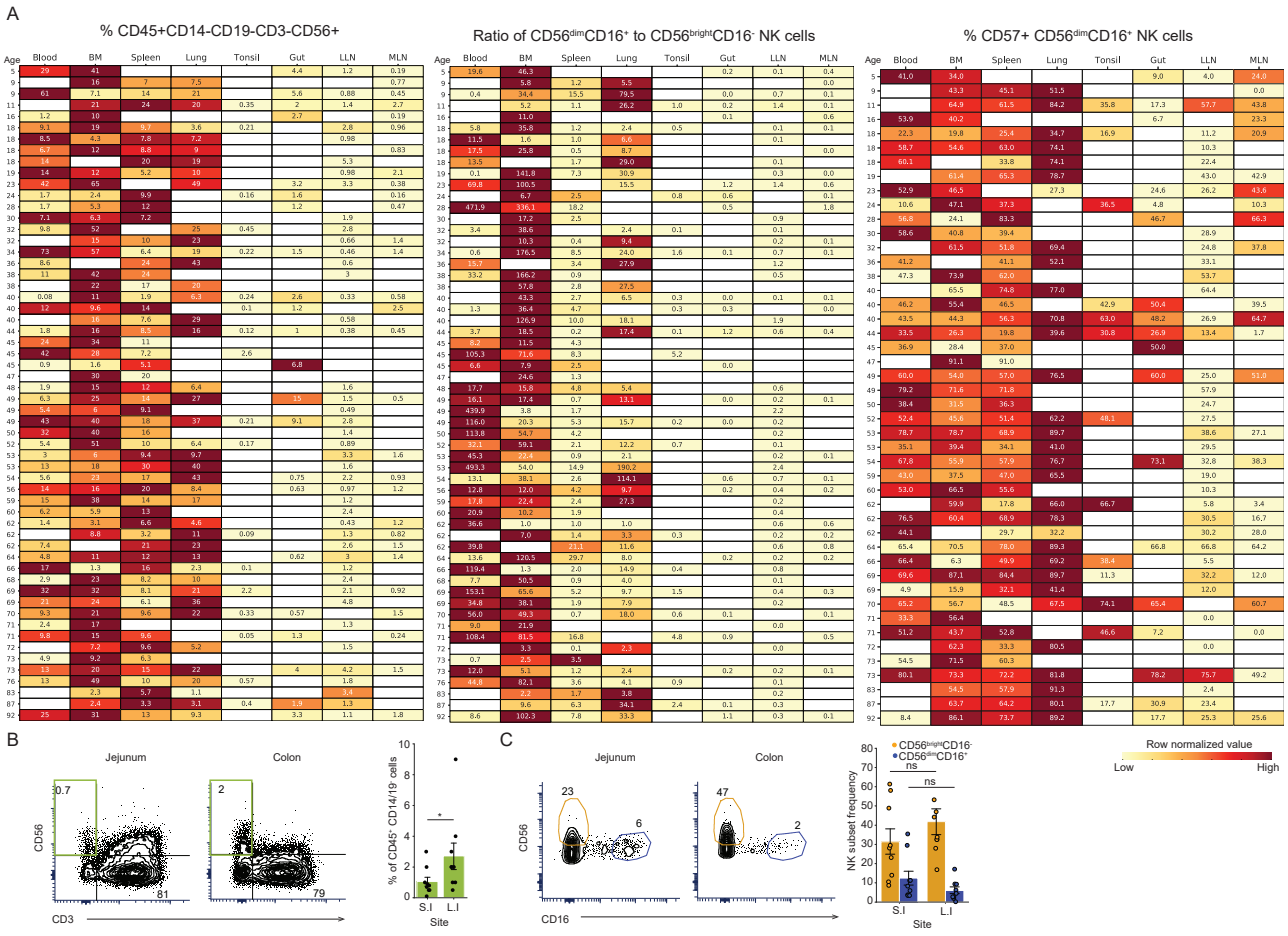

Figure S1. NK Cell and Subset Distribution in Different Tissue Sites, Related to Figure 1

(A) Heatmaps showing frequency of NK cells (left), ratio of $CD56^{dim}CD16^{+}$ to $CD56^{bright}CD16^{-}$ NK cells (middle) and frequency of $CD57^{+}CD56^{dim}CD16^{+}$ NK cells in blood and tissue sites for each individual donor reported in this study. Donors are arranged by increasing age and color intensity of each cell is based on row normalization of (min-max scaled) values. White cells indicate that no sample was obtained for a given donor.

(B) Representative flow plots showing NK cell frequency (top left quadrant) in small and large intestine sites reported in this study on left, and on right bar plots showing data compiled from 9 donors.

(C) Representative flow plots showing NK cell subset frequency in small and large intestine sites reported in this study on left, and on right bar plots showing data compiled from 9 donors.

Error bars represent ± SEM, *p $\leq$ 0.05; ns, non-significant. BM, bone marrow; LLN, lung draining LN; MLN, mesenteric LN.

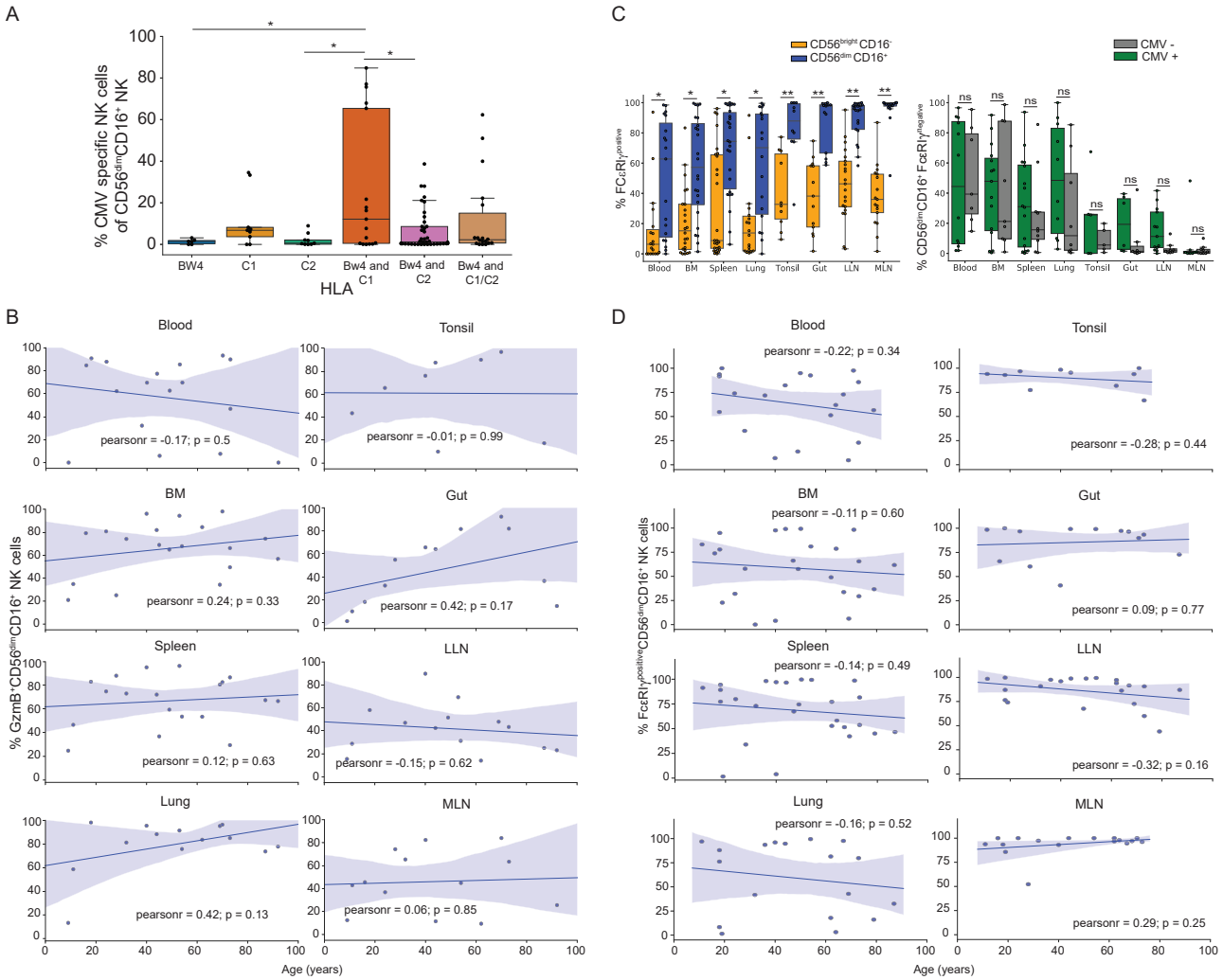

Figure S2. Distribution of NK Cell Functional Subsets Based on CMV Exposure and Age, Related to Figures 2 and 3

(A) Boxplot showing frequency of CMV-responsive ($CD56^{dim}CD16^{+}CD57^{+}NKG2C^{+}$) NK cells compiled from blood, BM, spleen, and lung from donors of indicated HLA types.

(B) Scatterplots showing the line of best fit for the frequency of $GzmB^{+}CD56^{dim}CD16^{+}$ NK cells in each tissue site as a function of age; pearsonr indicates the Pearson correlation coefficient for the comparison.

(C) Boxplot of compiled data from 10-24 donors showing the distribution of FcεRIγ-expressing NK cell subsets in different sites (left), and the frequency of $FcεRIγ^{negative}CD56^{dim}CD16^{+}$ NK cells between CMV -seronegative and -seropositive donors in different sites (right). $^{**}p \leq 0.01$, $^{*}p \leq 0.05$; ns, non-significant.

(D) Scatterplots showing the line of best fit for the frequency of $FcεRIγ^{+}CD56^{dim}CD16^{+}$ NK cells in each tissue site as a function of age; pearsonr indicates the Pearson correlation coefficient for the comparison.

Dots on the boxplots show data collected for each individual donor. BM, bone marrow; LLN, lung draining LN; MLN, mesenteric LN.

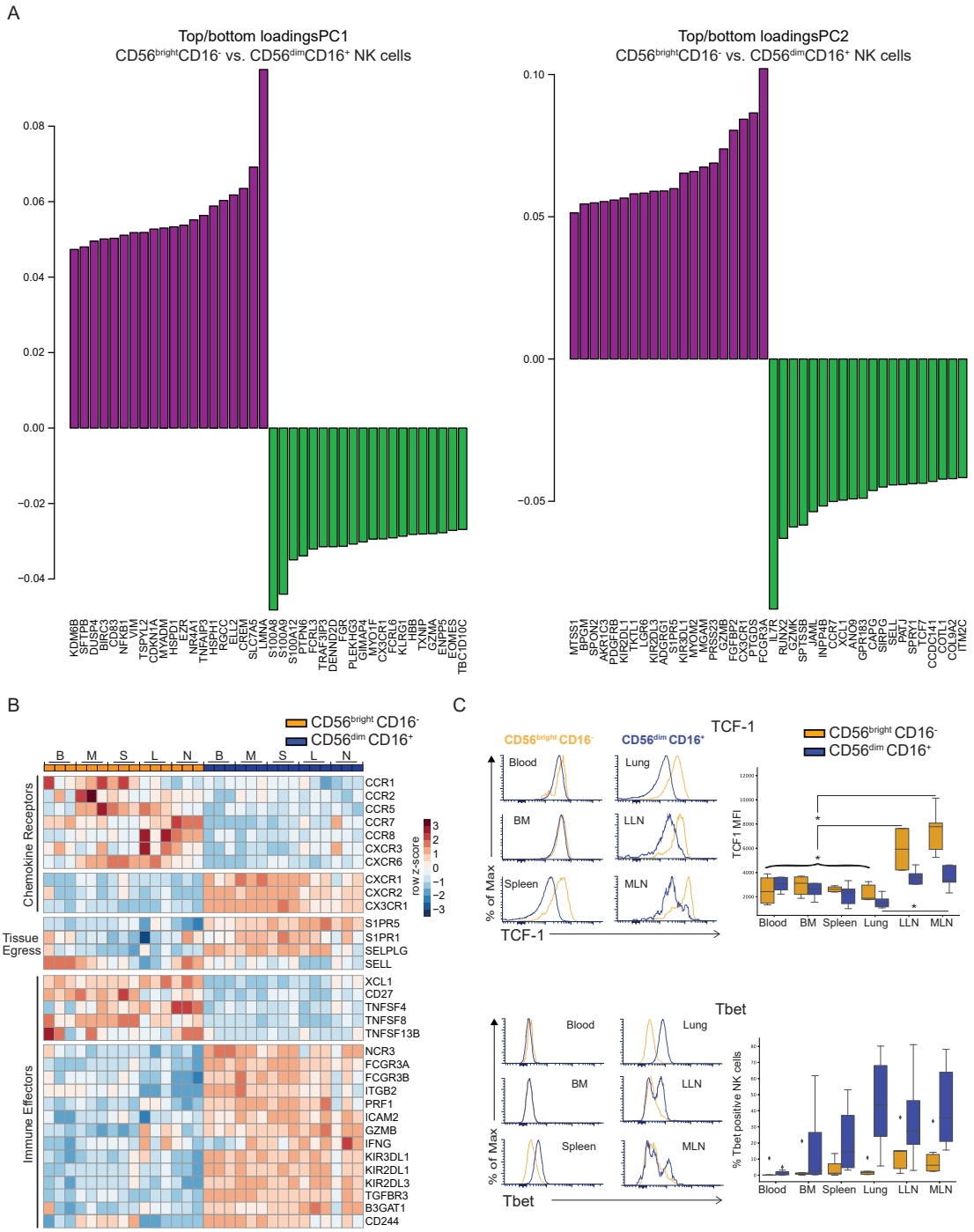

Figure S3. Differential Expression of Genes and Transcription Factors between CD56^{bright}CD16^{-} and CD56^{dim}CD16^{+} NK Cells, Related to Figure 4

(A) Bar plots showing highest/lowest loadings of principal component 1 and principal component 2 for PCA analysis comparing the global transcriptome of CD56^{bright}CD16^{-} and CD56^{dim}CD16^{+} NK cells in Figure 4A.

(B) Heatmap showing the differential expression of selected genes between CD56^{bright}CD16^{-} and CD56^{dim}CD16^{+} NK cell subsets isolated from 5 sites (B = Blood, M = Bone marrow, S = Spleen, L = Lung and N = LLN) from 3 donors.

(C) Representative histograms and boxplot of compiled data from 5 donors showing TCF1 (top) and Tbet (bottom) expression in NK cells subsets in different anatomical sites.

*p $\leq$ 0.05. Diamonds represent outliers in the data. BM, bone marrow; LLN, lung draining LN; MLN, mesenteric LN.

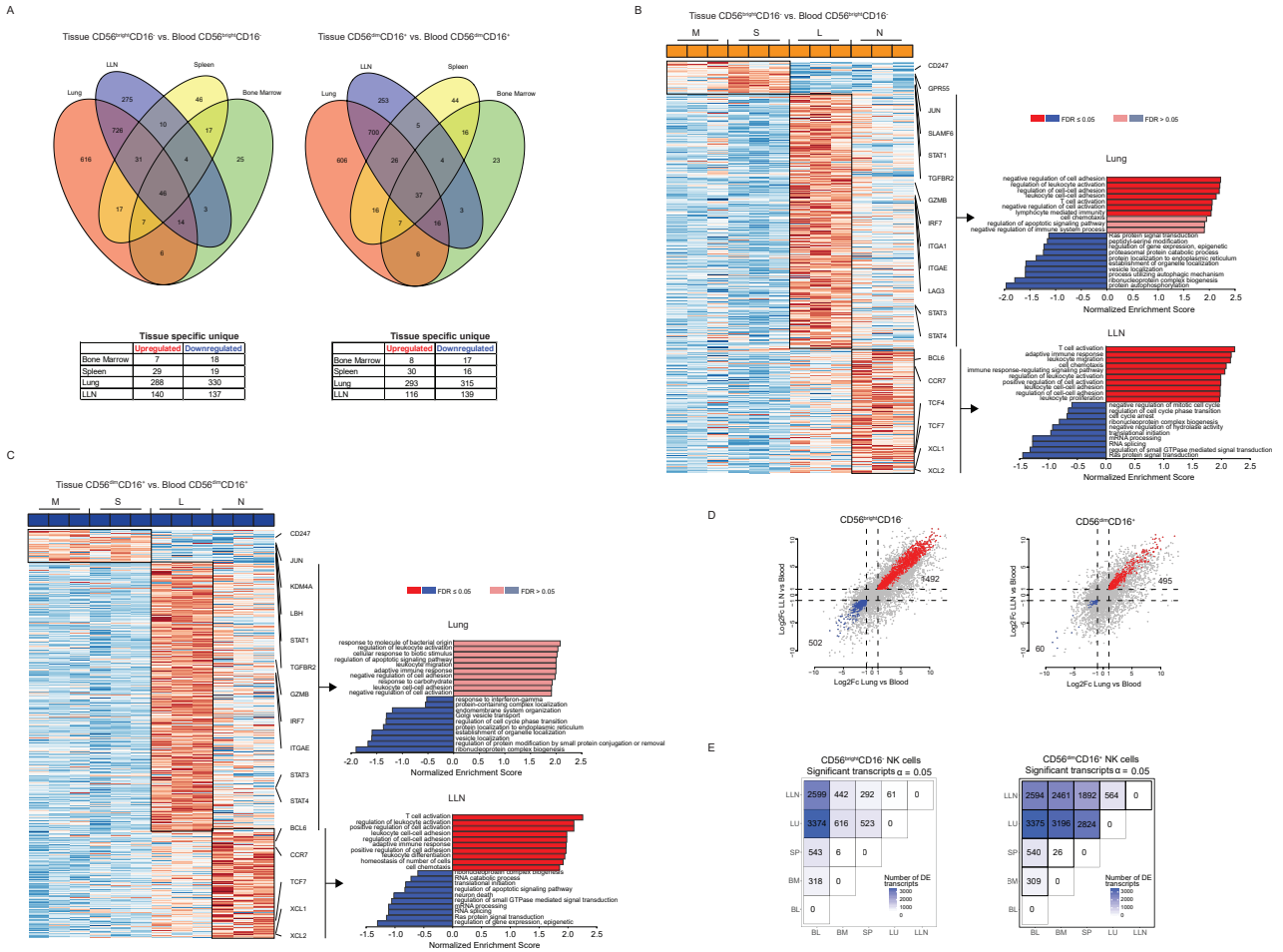

Figure S4. Tissue-Specific Transcriptional Programs for CD56^{bright}CD16^{-} and CD56^{dim}CD16^{+} NK Cells, Related to Figure 4

(A) Venn diagrams identifying unique differentially expressed (DE) genes between tissue CD56^{bright}CD16^{-} and blood CD56^{bright}CD16^{-} NK cells (top left) and tissue CD56^{dim}CD16^{+} and blood CD56^{dim}CD16^{+} NK cells (top right); table shows unique upregulated and downregulated genes for tissue CD56^{bright}CD16^{-} NK cells (bottom left) and tissue CD56^{dim}CD16^{+} NK cells (bottom right).

(B) *Left:* Heatmap shows upregulated genes in CD56^{bright}CD16^{-} NK cells in indicated sites. *Right*: graph shows pathways enriched in Lung and LLN CD56^{bright}CD16^{-} NK cells determined by GSEA. See Table S4.

(C) *Left:* Heatmap shows upregulated genes in CD56^{dim}CD16^{+} NK cells in indicated sites. *Right:* graph shows pathways enriched in Lung and LLN CD56^{dim}CD16^{+} NK cells determined by GSEA. See Table S5.

(D) Bi-plots for $\log_2$fold change (Fc) in gene expression for lung versus blood and LLN versus blood CD56^{bright}CD16^{-} NK cells (top) and lung versus blood and LLN versus blood CD56^{dim}CD16^{+} NK cells (bottom). Red dots represent genes similarly upregulated in both lung and LLN NK cell subsets (number in top right quadrant) and blue dots represent genes similarly downregulated in both lung and LLN NK cell subsets (number in bottom left quadrant).

(E) Matrix for the tissue wise comparison of transcriptional profile of CD56^{bright}CD16^{-} NK cells top and CD56^{dim}CD16^{+} NK cells bottom. Numbers in each box correspond to number of differentially expressed genes for each comparison. BL, blood; BM, bone marrow; SP, spleen; LU, lung; LLN, lung draining LN.

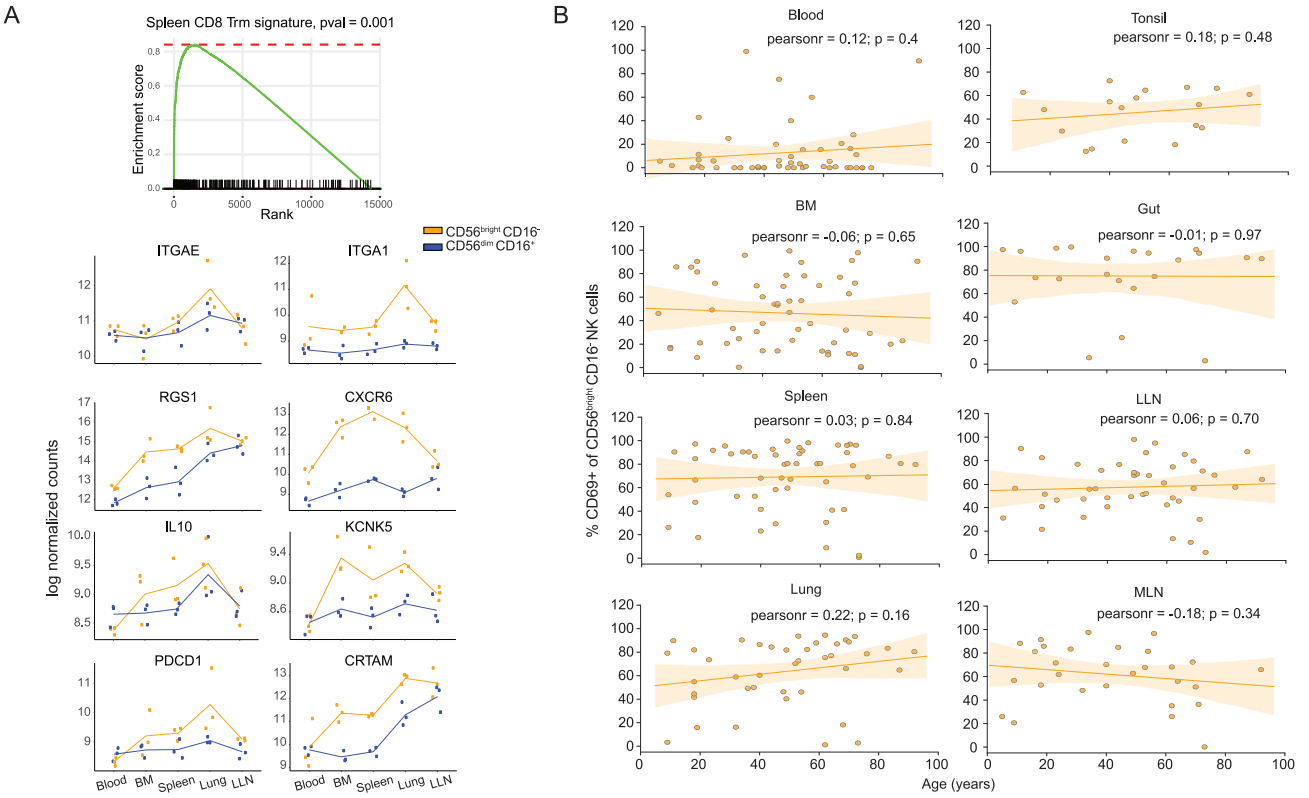

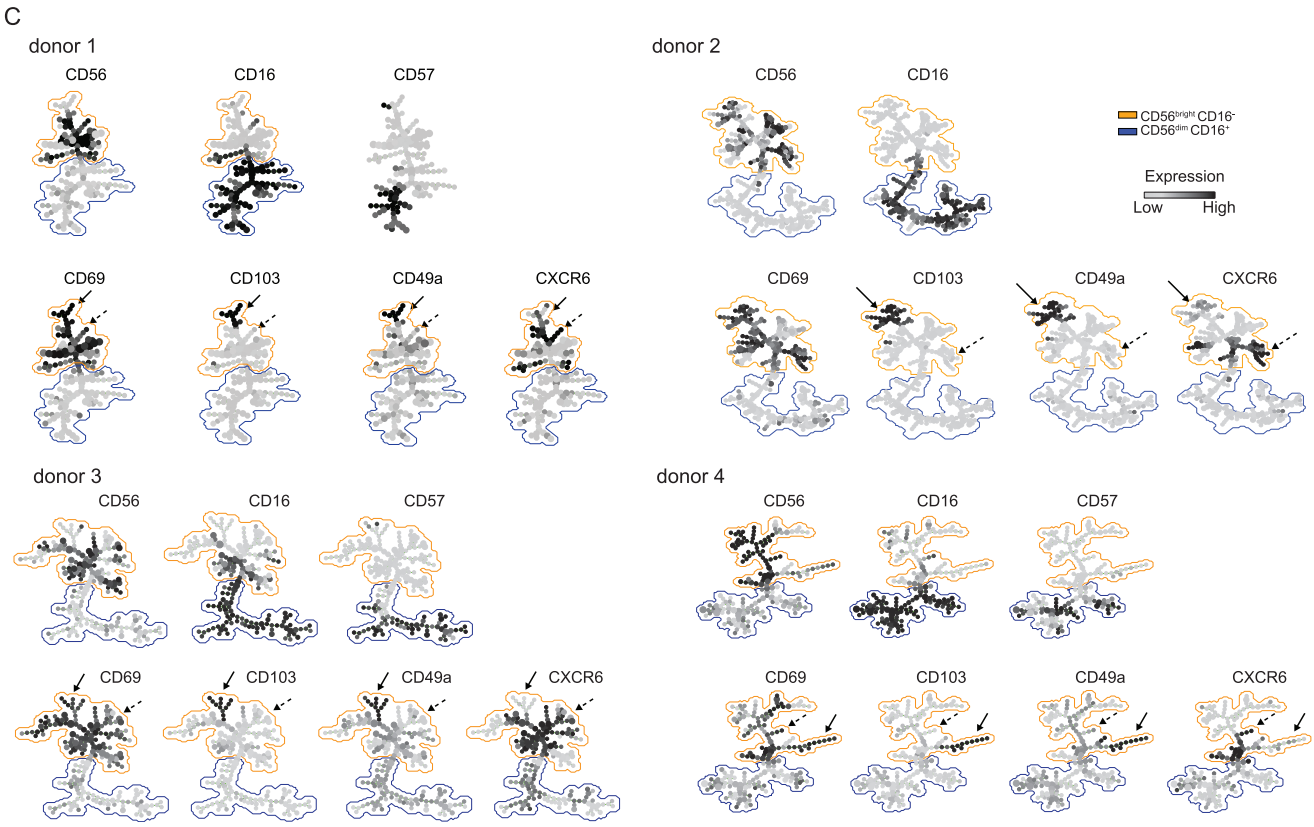

(legend on next page)

Figure S5. Transcriptional and Phenotypic Analysis of Tissue-Resident NK Cells in Different Sites, Related to Figures 5 and 6

(A) GSEA plot showing the enrichment of spleen CD8 tissue resident-memory T (Trm) gene signature within $CD56^{bright}CD16^{-}$ NK cells from all tissue sites (top) and scatterplots showing log normalized counts of key tissue-residence genes shown in Figure 5B heatmap (bottom). Dots show data for each individual sample and the line connects the mean value for each group of samples.

(B) Scatterplots showing the frequency of $CD69^{+}CD56^{bright}CD16^{-}$ NK cells in each tissue site as a function of age and line of best fit between the variables, pearsonr indicates the Pearson correlation coefficient for the comparison.

(C) Heterogeneity of trNK cells. SPADE plots for NK cells isolated from blood, BM, spleen, lung, gut, LLN, and MLN (donor 1) and from blood, BM, spleen, lung, and LLN for 3 additional donors (donors 2, 3, and 4). Solid black arrow identifies $CD103^{+}$ $CD49^{+}$ NK cells and dashed black arrow identifies $CXCR6^{+}$ NK cells. BM, bone marrow; LLN, lung draining LN; MLN, mesenteric LN

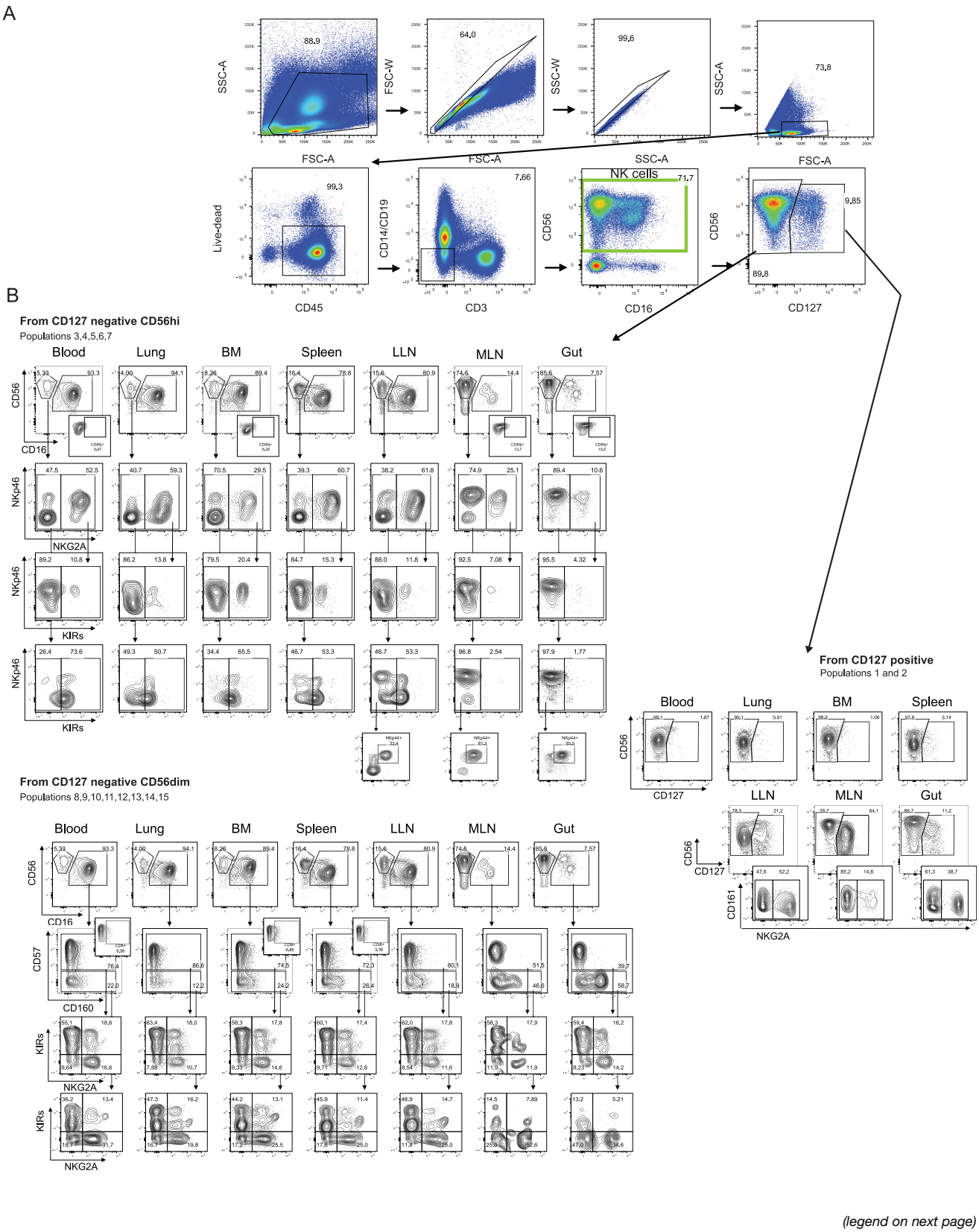

(legend on next page)

Figure S6. Gating Strategy and Representative Flow Plots for Clusters Identified by High-Dimensional Flow Cytometry Analysis, Related to Figure 7

(A) NK cells were identified as SSC-A^{low}CD45^{+}CD14^{-}19^{-}CD3^{-}CD56^{+} cells and used to carry out further analysis as described in materials and methods.

(B) Representative flow plots showing the expression of markers on NK cell clusters identified by high-dimensional analysis. BM, bone marrow; LLN, lung draining LN; MLN, mesenteric LN.

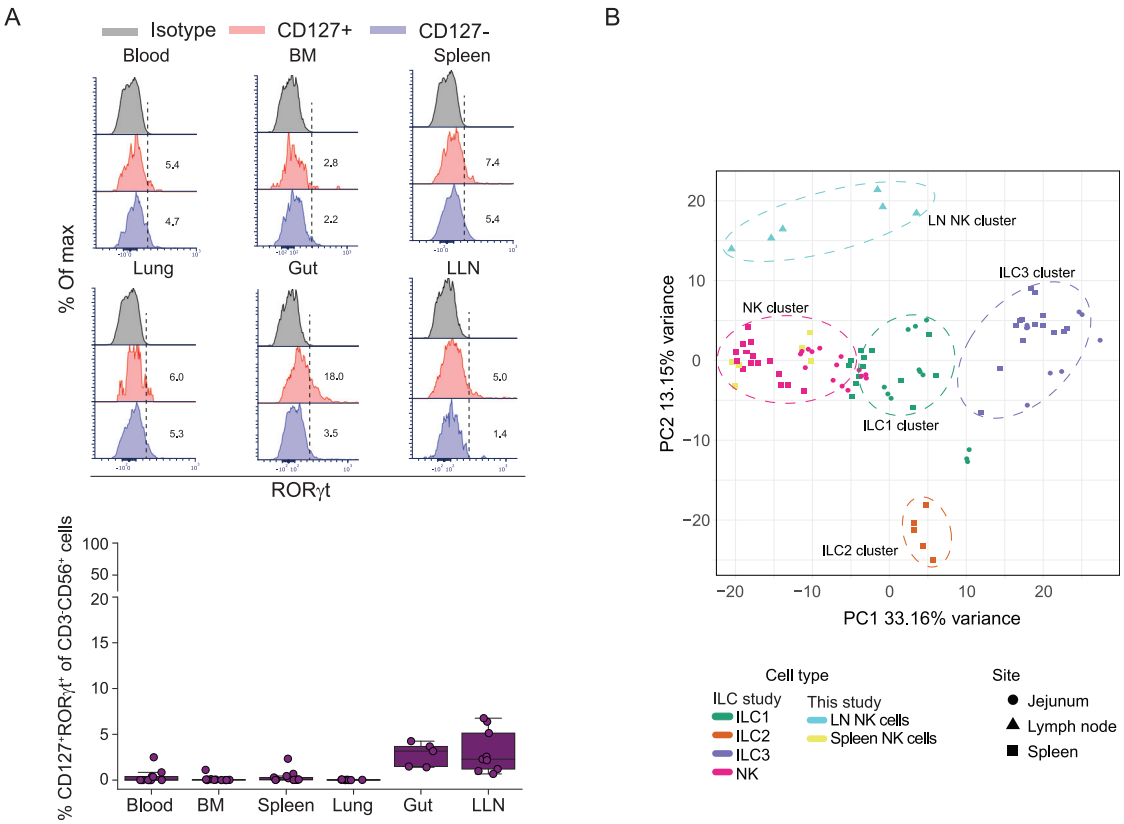

Figure S7. CD56^{bright}CD16^{-} NK Cells in Tissues Are Phenotypically and Transcriptionally Distinct from Known ILC Subsets, Related to Figure 7

(A) Representative histograms showing the expression of RORγt on CD127^{+} and CD127^{-} cells in blood and tissue sites on top, and on bottom boxplot showing the frequency of CD127^{+}RORγt^{+} cells of the total CD3^{-}CD56^{+} cells in blood and tissue sites compiled from 5-13 donors.

(B) PCA plot showing comparison of the transcription profile of NK cells from spleen (golden squares) and LLN (cyan triangles) from this study and NK cells and ILC subsets from spleen and jejunum from the ILC study (Yudanin et al., 2019). BM, bone marrow; LLN, lung draining LN; MLN, mesenteric LN.